The Use Of Low Amplitude Response Data For Seismic Capacity Assessment.

40 Wall Street • 19th Floor • New York, NY 10005

STRAAM Group, Inc.

High-amplitude and Low-amplitude Dynamic Measurements and Assessments.

Codes of practice and standards use much of their output for guidance on the design process. Notwithstanding this there is a little information about acceptable performance criteria, and such approaches as drift limits are widely used in seismic assessment. None of this addresses the state of health and the remaining capacity of a structure.

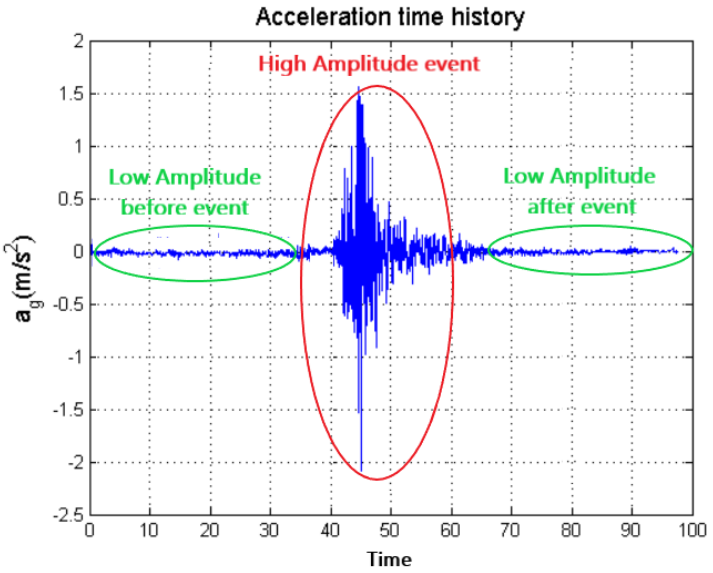

This paper introduces a different complementary method that addresses the current state of a structure without relying only on measurements at high amplitude. The diagram to the right demonstrates this concept. The response of a structure is shown before, during and after a seismic event. The suggested complementary approach uses a comparison of the 'before and after' dynamic behavior of the structure to assess its probable response to large events in the future. This complements the current method of analysis using data from the high amplitude event only. Also, it provides an economical alternative for all structures if they are not actively instrumented for high amplitude seismic monitoring.

There are several benefits to this approach:

1. Measurement of a structure's response at high amplitude is imprecise because of the short record-length, and several non-linearities involved. Details are considered below.
2. Assessment of the response at low amplitude carries a vast quantity of information about the state of a structure and of its capacity, if analyzed correctly.
3. Low amplitude data can be collected over long periods and this allows for precise and accurate measurement and analysis of the structure's characteristics.
4. Changes in the dynamic parameters reflect the effects of damage, or ageing in a structure and can be assessed accurately with longer data lengths.

A limitation of low amplitude measurement analysis is that no direct evidence of the behavior at high amplitude is included in the analysis. However, this can be overcome by using the same design process that is included in codes of practice and standards, but now having a calibrated structural definition in the elastic range. Extrapolation into ductile behavior can be performed exactly as currently conducted. The behavior of a structure at high amplitude is subject to a series of non-linearities, and measurement of this response together with the calibrated low amplitude behavior and the design assumptions for the ductile range,

potentially allow a greater understanding of the high amplitude response. Also, by combining the two approaches, a prediction combined with a calibrated measurement of actual performance is achieved.

The use of structural dynamic measurements is well established and can be used to define the system parameters by analysis of the modes of vibration that are inherent in the mathematical description of a structure.

Codes of practice do a very good job of establishing the magnitude and risk of a seismic event at a particular location, and this complementary approach does not change that, indeed it seeks to utilize the codification approach on top of the 'before and after' comparison.

The different approaches adopted by seismic, wind and mechanical engineers over the decades has been predicated on the data lengths commonly available. Each discipline can learn from others.

The important modal parameters used to describe a structure are:

- Frequency of resonance
- Modal damping ratio
- Deflected form of a mode of vibration (mode shape, also acts as an influence function)
- Displacement per unit force
- Participating mass

Interestingly, techniques for the measurement of structural dynamics parameters are considered in some detail in the document FEMA 461 (Interim testing protocols for determining the seismic performance characteristics of structural and nonstructural components, June, 2007) for shake table experiments. This paper extends these ideas to the full-scale, at the same time assessing the implications of the requirements for the analysis of randomly induced responses, necessary for statistically accurate parameter estimation.

High-amplitude techniques.

Earthquakes generally last for a few seconds to a few minutes, depending on the magnitude and distance of the event, providing a limited length of dynamic data for analysis. As a result, the currently used design approach is to combine the imposed force with the structural characteristics to produce a probable response. This process involves combining both force and response data, coupled with the use of 'most likely' values for ductility, energy dissipation, and acceptance of energy by the structure. In this approach, the incoming energy is assessed as having different energy levels at a spread of periods. In both mechanical and wind engineering, with longer lengths of data it is possible to use spectral techniques to establish structural parameters to a high degree of accuracy. In this way the characteristics of a structure, albeit in the elastic range, can be assessed with precision. This accurate characterization is very valuable in the seismic community. Attachment A contains a paper by Cruz and Miranda (2019) entitled, "Reliability of Damping Ratios Inferred from the Seismic Response of Buildings", which discusses some of the challenges in determining building modal periods of response and damping ratios from recorded earthquake strong-motion data.

1. **Structural modal period/frequency content of forcing** – In this section, we separate the structure's characteristics from the incoming seismic action and use the structural characterization to establish its condition. For a long time, the seismic force has been established by using a series of earthquake data from structures. Now, by using low amplitude data, very low noise instrumentation, and long data sets, we can separate the structural characteristics from the action caused by the seismic event. Mixing the

effects of the input action with the response causes a series of problems associated with structural identification. When the response of the structure is assessed at low amplitude, the modal parameters, including both long and short period resonances, can be assessed with high accuracy. This information is difficult to obtain from high-amplitude data because of the following:

(a) the short duration of high-amplitude events contributes to large variance errors in estimating building periods when using spectrally based analysis;

(b) the structural forces induced by ground motions reflect a combination of both the input forces and the structural response, as opposed to only the structural response;

(c) because of (b) above, the modal mass, the modal frequency and the modal and overall damping, represent a changed system that behaves as a larger system incorporating not just the structure, but also the adjacent ground.

(d) the input forces can be composed of quickly varying forces spread across a range of frequencies.

(e) the period of the structure changes when the amplitude of response is high. This can be caused by damage (in which the modal stiffness changes), by changes to structural damping and by changes of participating mass when soil-structure interaction occurs, (as in (c) above).

The foregoing implies that it is easier to measure the structural characteristics when soil/structure interaction is minimized. All of these factors contribute to significant challenges in determining the accurate modal periods of response of a building during high-amplitude recordings. As a result, high-amplitude techniques that experience these inherent difficulties yield varying levels of reliability of the results**.** This variability leads to a lack in confidence of the significance of the dynamic characteristic due to the difficulty of defining a parameter from a short data sample in which the parameter may change quite rapidly.

2. **Displacement** – Displacements are calculated from the high-amplitude events by analyzing the acceleration time history around the peak values of the event. Then the time history is filtered to the dominant frequency. Assuming simple harmonic motion (which is only a correct assumption if the frequency is invariant) the displacement is calculated using a double integration of the time history to simulate simple harmonic motion at a single frequency that may not represent the structural resonance. Yet the standard analysis provides a reasonable estimate based on the primary frequency. This leads to the imprecise estimation of peak displacements because of the behavior of the structure in short period modes of vibration.

3. **Damping** – Calculating damping from high amplitude events is fraught with difficulties, not just because of the short record lengths, but also, and crucially, because damping is a measure of energy dissipation, and the energy dissipation in the soil contributes. If techniques of estimating modal damping of the structure are used, there is also the factor of the non-linear behavior masquerading as an increase in damping if the measurement is based on averaging methods (such as using spectrum-

based methods, autocorrelation, or some time-stepping fitting methods). In the case of each of these methods there is an introduced bias that overestimates the value of damping. Fortuitously, there are now several methodologies for measuring non-linear damping directly from a time-history of response. The most important aspect of this analysis is that it becomes possible to establish the rate of change of damping with increasing amplitude. Nevertheless, for these methods to work accurately, long record lengths are required.

Calculating damping from a technique of system identification (as depicted in the attached Cruz and Miranda paper) in which a time history is artificially created and compared with the measured response. Parameters are then changed until a satisfactory fit is achieved. The resulting damping estimate contains influences from all the aforementioned mechanisms as well as the structural contribution. There are several parameters that must be modified including both the force and the damping, and an error in the estimation of one assumption, influences the other. This has led to skepticism about the ability to extract damping data from high amplitude responses.

It is common practice to assume, in seismic engineering design, that the structural component of damping may be assumed to be 5%, and that even if it is not, the calculation of displacement will still be quite accurate. Unfortunately, this is not true, and a small value of damping at low amplitude will result in a structure reaching high amplitude faster than expected, which in turn leaves it with inertia to overcome as well as the rising input forces.

Value of this approach - Regardless of the sources of error, the high-amplitude techniques provide valuable information for engineers to conduct analysis from the time history of an earthquake. Displacements are a critical criterion for determining the response from a seismic event and using the measurements can yield relatively accurate values. The use of these techniques in addition to the 'before and after' approach undoubtedly helps in establishing a complete picture of the structural behavior. A comparison of the response of the structure both 'before and after' a seismic event gives a comparison under similar conditions in which changes are a function of changes in the structure only.

Limitations to this approach – It is important to be aware that parameters may be changing rapidly through a seismic event, and that changes may appear to be changes in other parameters. This is a function of the short data lengths, and the non-linearities in both the structure and the incoming force. Thus, the variability of the dynamic characteristics erodes confidence in the accuracy of their estimation together with a lack of confidence in their true values. Traditional high amplitude equipment is not capable of capturing low amplitude response information, although some of the most modern devices, already deployed, may be usable for this complementary approach.

Low-amplitude techniques.

In both mechanical and wind engineering the response to random excitation has been studied for over four decades. By using low-amplitude measurements, the flexibility to measure the dynamic response can occur frequently, although times at which the wind is stronger, or traffic intensity is more severe allows the analysis to larger amplitudes of response, which in turn adds confidence to extrapolations to larger amplitudes within the elastic range. The analysis of the dynamic response information is based on the use of sufficient lengths of data to allow spectrally based analysis to reduce random variance errors to within a well-defined proximity to the average response to a mean wind speed. Wind engineers then have several techniques for estimating the

ratio of the peak response to the mean response. If the random data are well behaved, then this ratio is also well-behaved. This type of random response is defined as stationary, meaning that the statistical properties remain invariant with time. Thus, the system properties of the structure can be well defined with a high level of accuracy. These dynamic parameters vary little within the elastic range which applies here. The luxury of this type of analysis is not available for short data lengths associated with earthquakes but can be used to complement that approach. Therefore, these techniques provide the consistency needed to accurately define the dynamic parameters not available through seismic techniques.

1. **Frequencies of resonance** - Wind engineers refer to the inverse of the period of a structure as the frequency of resonance. By using the appropriate techniques for low-amplitude energy, estimating the structure's dynamic properties, including the frequencies of resonance, can occur to a very high level of accuracy (99%). Also, various structural modes of vibration can be identified allowing for clarity of the stiffness relationship throughout the structure. Further, the mode shapes are always consistent in the elastic amplitude range which is not necessarily the case with high-amplitude responses. By introducing a 'before and after' measurement of the response of a structure it is possible to establish the displacement per unit force through the measurement of the parameters which define the structure as a system. This is possible because 'before and after' an event the modal mass is invariant.

2. **Damping** – By using low-amplitude energy, the damping response is nearly 100% generated from the structural elements, and there is negligible contribution of the other mechanisms of damping such as radiation, hysteretic and viscous sources. As referenced in the paper, Attachment B, "Generalized Random Decrement Method for Analysis of Vibration Data", the Random Decrement Algorithm allows for measuring the structural damping response to a very high level of accuracy, generally better than 98% accurate when measuring structural modes of vibration. *Because it is not common practice to separate structural damping from overall damping in the seismic design process the importance of the information available from the non-linear structural damping parameter may not be immediately obvious in the communities working with seismic design.* Measuring 'structural' damping accurately is a critical aspect of defining the structure's dynamic properties and cannot currently be achieved accurately using high-amplitude data sets. The Random Decrement (RANDEC) algorithm gives an amplitude dependent curve that can give critical insight into how the structure functions over a wide range of amplitudes. RANDEC was developed by NASA to detect early stage damage in the wings of the space shuttle, and if used appropriately, provides an accurate change in response due to damage to the structure. This parameter is extremely sensitive to changes in energy dissipation within the structure, such as that caused by damage.

Value to this approach – The use of low-amplitude techniques allows measurements to be taken almost any time since there is normally movement of the structure from ambient sources of excitation. So long as measuring equipment has a low noise platform, then very low amplitude responses can be captured. Because even these amplitudes represent motion in the linear-elastic range then extrapolation throughout that range is justified (and supported by experiment). This provides flexibility and consistency for taking dynamic response measurements, and these measurements can be captured at almost all times, leading to an accurate assessment of the system properties. The frequency response is accurate to within 99% and structural (non-linear) damping values can be estimated to better than 98% precision using these techniques. This high level of accuracy allows a precise comparison of the 'before and after' system properties, including their non-linear aspects. In this way the estimation of structural parameters becomes consistent and accurate.

The equipment necessary for the capture of low amplitude responses can also be used to capture the high amplitude response. The inverse is not normally true, and so there is an added advantage to using these new techniques.

Limitations to this approach – The establishment of structural identification through the use of low amplitude techniques requires extrapolation throughout the elastic range, and then beyond. The behavior of the structure at low amplitude can be used for calibration purposes, and then extrapolations within the ductile range must use conventional design assumptions.

Value in combining both high-amplitude and low-amplitude techniques.

Using both techniques provides a very clear picture of the performance of a structure as it transitions through a high-amplitude event:

Before event – Using low-amplitude dynamic analysis techniques prior to a high-amplitude event would establish the baseline measurement of a structure's dynamic characteristics and response. It allows the comparison of the structure's description with what is expected in the design philosophy. Additionally, it can be used to establish the decreased capacity associated with ageing of the structure. These measured structural parameters establish a baseline condition and can be used for future comparison to quantify damage to a high degree of accuracy.

During the event – Analysis of the high-amplitude event gives an opportunity to establish the most likely velocity and displacement behavior during the high amplitude event, and these estimates give a good insight into the probability of damage having occurred. However, the information is important to understand how a structure responds to the imposed forces.

After event – Taking a follow up post-event measurement of the dynamic properties provides a comparison of the any changes to the state of the structure. Changes to mode shapes can indicate an area of weakness, changes to the frequency of resonance indicate a change of modal stiffness, and changes to structural damping indicate changes to the energy dissipation of the structure (such as those caused by cracking or other damage). The structural damping parameter is extremely sensitive to damage, often 10 to 20 times more sensitive than changes in stiffness.

References

Cruz, Cristian, and Miranda, Eduardo, 2019, Reliability of damping ratios inferred from the seismic response of buildings, *Engineering Structures*, Volume 184, pages, 355-368.

Spano, P.D. and Zeldin, B.A., 1998, Generalized Random Decrement Method for Analysis of Vibration Data. Journal of Vibration and Acoustics, Volume 120

Attachment A:

Engineering Structures 184 (2019) 355–368

Contents lists available at ScienceDirect

Engineering Structures

journal homepage: www.elsevier.com/locate/engstruct

Reliability of damping ratios inferred from the seismic response of buildings

Cristian Cruz[a,b,*], Eduardo Miranda[b]

[a] Departamento de Obras Civiles, Universidad Técnica Federico Santa María, Santiago, Chile
[b] Department of Civil and Environmental Engineering, Stanford University, Stanford, CA 94305-4020, United States

ARTICLE INFO

Keywords:
Damping ratios
Reliability
Damping of higher modes
System identification

ABSTRACT

This paper studies the reliability of damping ratios inferred from the seismic response of buildings employing a modal minimization parametric system identification technique. The reliability of inferred damping ratios is quantified through the use of three metrics: (1) dynamic amplification factors; (2) Arias modal contribution factors; and (3) reliability intervals. Dynamic amplification factors measure the amplification of 1% damped floor acceleration spectral ordinates of the recorded response at the roof in the vicinity of identified modal periods with respect to those of the motion recorded at the base of the building. It is shown that this metric allows to determine if the earthquake produced a minimum dynamic amplification of the first and second modes of the structure, to reliably identify their damping ratios. The Arias modal contribution provides a measure of the intensity of a computed modal response relative to the total predicted structural response. It is argued that only damping ratios from modes with a minimum contribution to the seismic response may be reliably estimated. The third metric corresponds to the reliability intervals of the identified damping ratios, which measure the sensitivity of the objective function to small variations in the damping ratio. It is shown that the objective function is typically significantly less sensitive to variations in damping ratios than to similar variations in modal periods, which leads to larger variability in the results for damping with respect to that obtained in modal periods. Reliability screening tests are developed based on establishing limiting values for these three metrics. It is shown that these screening tests are capable of discriminating inferred damping ratios that are reliable from those that are not, independently from the adopted identification technique, and also reducing the variability of the inferred results.

1. Introduction

The inherent damping of a building is usually modeled as linear viscous, as it is a simple mathematical representation of all the sources of energy dissipation in a structure that are not explicitly included in the structural model. These sources include, among others, the inherent damping capacity of the building materials, the energy dissipation due to friction between the different structural and non-structural elements (or within them), the energy dissipated due to soil-structure interaction, and the effects of the aerodynamic properties of the building [1]. Even though there is evidence that some of these sources of energy dissipation do not behave in a viscous manner, assuming linear viscous damping has become the standard in current structural analysis methods because it significantly simplifies the differential equations of motion (e.g., [2,3]) but, more importantly, because multiple studies have shown that employing this damping model in buildings responding elastically allows to adequately reproduce the measured response of instrumented buildings (e.g., [4–8]). Therefore, for many years the most commonly used approach to model damping in structures responding elastically has been to group the contribution of the various sources of energy dissipation - whose modeling may be impractical, too complex, or not yet fully understood - using a linear viscous damping model. Given that it is not possible to measure damping directly, the most reliable way to determine its value in existing buildings is by using system identification techniques to infer it from measured dynamic responses.

Since the late 1970s, the field of structural identification has shifted emphasis from non-parametric to more complex mechanical parametric methods since they provide a better understanding of the mechanics of the structure and because of the availability of faster computers [9]. A parametric system identification technique consists in finding the optimal set of parameters to be used in a numerical model of the structure in order to reproduce the recorded response with the least error. The main advantage of using a parametric model system identification technique is that a structural model is used, which allows the computation of response parameters not directly measured, such as lateral

* Corresponding author at: Departamento de Obras Civiles, Universidad Técnica Federico Santa María, Santiago, Chile.
E-mail addresses: cristian.cruzd@usm.cl (C. Cruz), emiranda@stanford.edu (E. Miranda).

https://doi.org/10.1016/j.engstruct.2019.01.056
Received 2 January 2018; Received in revised form 22 December 2018; Accepted 14 January 2019

displacements, interstory drifts, story shears, story overturning moments, etc. These techniques also allow to understand the influence of the parameters being inferred/identified on response parameters not measured, providing an improved understanding of the seismic response of the building. It should be stressed that models per se are not identifiable, but rather what is identified are the best set of parameters of the selected model that minimize a measure-of-fit between the recorded response and the response computed with a model. Different parametric system identification methods differ primarily in the numerical model of the building, the definition of the objective function used to quantify the difference between the measured response and that predicted by the numerical model, and the algorithm employed to perform the optimization (e.g., [10–14]). Another differentiating factor of different system identification techniques is whether the input to the system is known or not. The field of Experimental Modal Analysis (EMA) deals with methods that require knowledge of the input signal – in the case of earthquake engineering, the input ground motion, – and most studies attempting to identify structural properties from earthquake records fall into this category (e.g. [6–8,10,11,15–18]). The field of Operational Modal Analysis (OMA) regards those methods where the input signal is unknown. Recent investigations in this field show promising applications to the field of earthquake engineering (e.g. [19–25]), especially when strong soil-structure interaction effects – that might distort the input signal – are considered.

Structural models are an idealized mathematical description of the motion of a building. In practice, several simplifying assumptions of the selected model, such as linear-elasticity, time invariance, fixed condition at the base, linear viscous damping behavior, etc., are not entirely satisfied. Consequently, the numerical model will never be able to perfectly reproduce the measured structural response even if the response is linear. In other words, there will always be an error in the prediction, introducing uncertainty about the true values of the identified parameters. In addition to the system identification method used to infer damping ratios, variability (and therefore uncertainties) in inferred damping ratios are influence by many other factors such as accuracy of the sensors, limited number of records or malfunction in certain recording channels, limited duration of response, noise level in the recorded acceleration time histories, modal response not sufficiently excited or not sufficiently contributing to the total recorded response, etc. Therefore, for a given building, identified damping ratios may exhibit variations from one earthquake to another, particularly for certain modes. Several investigations have dealt with the uncertainty of the estimated parameters, most of which are based on a probabilistic approach. One of the first works on this subject is the one by Gersch [26], who employed the Cramer-Rao lower bound theorem to develop expressions for the maximum achievable accuracy of the modal frequencies and damping ratios inferred by a method based on the maximum-likelihood estimates of an auto-regressive model [27]. More recent studies have taken similar approaches, leading to the conclusion that the uncertainty in the identified damping ratios is significantly larger than in the identified modal periods (e.g., [18,28–30]). It should be noted that this observation was first made much earlier by several researchers using non-probabilistic approaches, such as McVerry [5] and Beck and Jennings [10].

A system identification technique may infer an important number of parameters by using recorded response. However, not all inferred values may be reliable. For example, in buildings the product of the modal participation factor and modal shapes decreases rapidly with increasing mode. Therefore, the contribution of higher modes to the total recorded response tends to decrease as the mode number increases. This means that there is a need for cut-off criteria for inferred parameters that may not be reliable because they correspond to modes of vibration that do not significantly contribute to the total response. But unreliable inferred modal properties may also occur for lower modes. For example, in small magnitude earthquakes the first mode may not be sufficiently excited, and even though the product of the modal participation factor and modal shape for the first mode may be large the modal response may be almost negligible or have a small signal to noise ratio as noise tends to be larger for low frequencies in acceleration sensors leading the system identification technique to infer some values, but they may not be reliable. In these cases, in addition to quantifying the variability in the inferred damping ratios it is necessary to discriminate which values are reliable and from those which are not.

This study is part of an investigation aimed at evaluating damping ratios inferred from the seismic response of buildings. In a first paper, the authors evaluated the damping ratio of tall buildings for both the fundamental and higher modes of vibration [8]. The paper showed that damping ratios tend to decrease with increasing building height, and that, once a threshold level of response is exceeded, damping ratios remain approximately constant with increments in seismic response as large are five- or ten-fold, provided that the building remain elastic or nearly elastic. In a second paper, the authors analyzed a larger dataset of buildings in order to provide damping recommendations for higher modes [7]. That study showed that damping ratios of higher modes are typically larger than those of fundamental modes of vibration and that damping ratios of higher modes increase approximately linearly with increasing frequency. This paper is aimed at developing metrics to examine the reliability of the inferred modal damping ratios based on (1) the capacity of the ground motion to excite the modes being identified; (2) the relative contribution of the different modes to the total seismic response; and (3) the sensitivity of the computed structural response to changes in modal damping ratios. Based on these concepts, which are familiar to most structural engineers, a series of metrics are developed to quantify the reliability of the damping ratios, and to develop screening tests to identify inferred damping ratios that are not reliable by imposing limiting values on these metrics.

2. Variability in identified parameters

There are many available different system identification techniques to infer dynamic properties of buildings from seismic records. In some cases, for the same building and for the same earthquake, different investigators using different system identification techniques may result in different results. In order to illustrate this situation, this section presents results of inferred dynamic characteristics for three buildings obtained by different investigators to show that identification of damping ratios is more challenging than identifying modal frequencies. Please note that the details of the system identification techniques employed by these different investigations are not the focus of this section. The interested reader can go to the cited papers for details about them, or to Section 3 for details about the technique employed in this investigation. The main question that is discussed in this section is the following: Why identifying damping ratios is harder than identifying periods? Although this is also related to the particular system identification method used, the main reason is that the seismic response of buildings is more sensitive to changes in modal frequencies than it is to changes in modal damping ratios and therefore there is a much smaller variability in identified modal frequencies than in inferred modal damping ratios.

The first building corresponds to the 1900 Avenue of the Stars building located in Los Angeles, California (Fig. 1, left). The building has height of 113 m, with 27-stories above ground level and one basement. It has a rectangular shape of 63 m by 33 m, and its lateral resistant system consists of steel moment-resisting frames. This buildings was designed in 1969, and instrumented since its construction. The structural response during the 1971 San Fernando earthquake was captured by sensors in the building. This was one of the first buildings whose response was recorded during an earthquake, so it captured the interest of people working on system identification at the time. Among these researchers were Hart and Vasudevan [31], and McVerry [5], who analyzed the building using two different techniques. Hart and Vasudevan used a simplified method based on the peaks of the roof-to-

Fig. 1. Left: 1900 Avenue of the Stars building. Center: Pacific Park Plaza building. Right: Embarcadero Building (all images from Google Maps, 2016).

ground transfer function, McVerry used a parametric modal minimization technique in the frequency domain. For this investigation, all the buildings were analyzed using the parametric modal minimization method in the time domain described in Section 3.

The second building to compare is the Pacific Park Plaza building, located in Emeryville, California (Fig. 1, center). This building was built in 1983, and has 30 stories with a total height of 95 m. The building has a Y shape in plan and has shear walls from the foundation to the second floor at the central core and at the three wings. Above the second level, the lateral resistant system consists of ductile moment resistant reinforced concrete frames. The building was instrumented in 1985 by the United States Geological Survey, with 21 channels distributed in the 30th, 21st, 13th, and ground floors. The building was shaken by the 1989 Loma Prieta earthquake, and its recorded response has been used by several researchers to infer its dynamic properties. The most relevant studies on this building correspond to Celebi [16], and Safak and Celebi [15]. Both studies use a discrete time linear filters method for system identification [12]. Reinoso and Miranda [32] also studied this building using the parametric modal minimization method in the time domain, however, they used a simplified continuous cantilever beam model as the structural model and further simplified the model by constraining the damping ratios to be equal for all modes, as they were primarily interested in estimating acceleration demands in buildings with only three parameters: fundamental period T_1, damping ratio ξ, and lateral stiffness ratio α.

The third building is one of the buildings of the Embarcadero Center, located in the financial district of San Francisco, California (Fig. 1, right). The building has 47 stories above ground level and two basements, with a height of 172 m. The lateral resisting system consists of steel moment-resisting frames in the longitudinal direction and a dual system that combines moment-resisting frames and eccentrically-braced frames in the transverse direction. The building has an approximately rectangular plan shape, with setbacks in the transverse direction at levels 39 and 41. The building was constructed in 1978, and instrumented in 1985 with 18 accelerometers on 7 levels. The recorded response of this building during the 1989 Loma Prieta earthquake was studied in the previously mentioned studies of Celebi [16], and Reinoso and Miranda [32]. It was also more recently studied by Bernal et al. [18], who used a subspace method to perform the system identification.

Tables 1–3 show the results obtained by all the aforementioned investigators for the damping ratio and period of the fundamental mode of all the buildings – in both directions. The tables also indicate the difference in the identified properties with respect to those obtained in this investigation. Even when the different investigations use the same data, it can be seen that there is significant variability in the results. The variability, however, is several times higher for the inferred damping ratios than for the inferred fundamental periods. Taking the results from this investigation as a reference, the average difference in periods is only 1.9%, with a standard deviation of 2.5%. However, for damping

Table 1
Results for 1900 Avenue of the Stars.

Study	T_1 [s]	Diff.*	ξ_1 [%]	Diff.*
N-S Direction				
Hart and Vasudevan [31]	4.26	−2.5%	5.2	15.6%
McVerry [5]	4.37	0.0%	4.4	−2.2%
This investigation	4.37	–	4.5	–
E-W Direction				
Hart and Vasudevan [31]	4.27	0.9%	6.5	160.0%
McVerry [5]	4.23	0.0%	2.2	−12.0%
This investigation	4.23	–	2.5	–

* Difference with respect to this investigation.

Table 2
Results for Pacific Park Plaza.

Study	T_1 [s]	Diff.*	ξ_1 [%]	Diff.*
N-S Direction				
Celebi [16]	2.63	−2.2%	11.6	75.8%
Safak and Celebi [15]	2.50	−7.1%	13.0	97.0%
Reinoso and Miranda [32]	2.60	−3.3%	6.0	−9.1%
This investigation	2.69	–	6.6	–
E-W Direction				
Celebi [16]	2.63	−3.3%	15.5	162.7%
Safak and Celebi [15]	2.50	−8.1%	13.0	120.3%
Reinoso and Miranda [32]	2.60	−4.4%	4.0	−32.2%
This investigation	2.72	–	5.9	–

* Difference with respect to this investigation.

Table 3
Results for Embarcadero Building.

Study	T_1 [s]	Diff.*	ξ_1 [%]	Diff.*
N-S Direction				
Celebi [16]	5.26	0.0%	2.5	92.3%
Reinoso and Miranda [32]	5.3	0.8%	2.5	92.3%
Bernal et al. [18]	5.26	0.0%	1.4	7.7%
This investigation	5.26	–	1.3	–
E-W Direction				
Celebi [16]	6.25	0.3%	3.7	94.7%
Reinoso and Miranda [32]	6.25	0.3%	1.0	−47.4%
Bernal et al. [18]	6.25	0.3%	1.7	−10.5%
This investigation	6.23	–	1.9	–

* Difference with respect to this investigation.

ratios, the average difference across buildings is 64.5%, with a standard deviation of 54.9%. In other words, there is a general agreement on what is the fundamental period of these structures - with discrepancies that are within a tolerable margin - but are larger differences on the damping ratios. Moreover, without further analysis, it is not possible to tell which of the reported damping ratios is closer to the true value for the different buildings.

There are several questions that arise from this simple comparison exercise: Why it is easier to identify periods than damping ratios? Which of these reported damping ratios is more reliable? Is it possible to define an interval that is likely to bracket the true damping ratio of the building? This paper addresses these questions. The reliability is estimated based on the level of modal excitation, the relative contribution of the different modes to the structural response, and on the sensitivity of the objective function to small changes in damping ratio. Metrics to quantify the reliability of the inferred damping ratios are then developed, and a series of reliability tests are proposed. Finally, an example of the different reliability tests is presented using the actual records of a 32-story building subjected to 8 different earthquakes.

3. System identification: parametric modal minimization in the time domain

The modal minimization method is a parametric system identification technique that consists in finding the optimal set of parameters that will make a mathematical model of the structure reproduce the recorded response with the least error. The fit can be done in either time domain (e.g., [10]) or in frequency domain (e.g., [11]), without significant differences in the results when the same building model is used and the response is entirely elastic. If this method is combined with a modal response-history analysis, then the modal parameters that are identified directly correspond to the modal damping ratios, modal periods, and products of mode shapes and modal participation factors that an engineer should use in order to reproduce as best as possible the recorded response of the building. In other words, it has the advantage that the method of analysis used in the system identification is the same as the most commonly used method to analyze buildings in current engineering practice, that is, a linear elastic classic modal analysis. For this reason, it was the method chosen for this investigation. Here, the process was carried in the time domain, adapted from [10], because when used in the frequency domain it may lead to overestimation of damping ratios in the presence of even mild nonlinearities, even if this occurs in a short segment of time in the record.

The first step is to define a mathematical model of the structure. The second step is to find the parameters that minimize the error of the response predicted by this model. The objective function J is defined as the least-squares difference between the recorded relative acceleration $\ddot{u}$ and the one predicted by the model $\hat{\ddot{u}}$, normalized by the recorded relative acceleration:

$$J(\theta) = \sum_{j=1}^{N_{sen}} \sum_{i=1}^{\tau} \frac{[\ddot{u}_j(i\Delta t) - \hat{\ddot{u}}_j(i\Delta t)]^2}{\sum_{k=1}^{\tau} [\ddot{u}_j(k\Delta t)]^2} \tag{1}$$

where θ is the set of parameters that govern the mathematical model of the structure, N_{sen} is the number of sensors above ground, τ is the length of the digital records, and Δt is the time step of the records. This objective function provides an overall measure of fit between the computed and measured relative accelerations across all the record and giving equal weight to all sensors. The purpose of the normalization of the squared error at each sensing location by introducing the denominator in Eq. (1) is to provide an equal weight to each sensor location. Please notice that if this normalization is not used, the system identification would converge toward parameters that minimize the difference between computed and measured relative accelerations in sensor locations experiencing larger relative accelerations which tend to increase with increasing height and therefore, in general, would tend to produce better fits for sensors located higher in the building than those in the lower part of the building. The system identification problem then consists in finding the optimal set of parameters θ, that minimize J.

In this work, a linear-elastic model, considering classical damping (i.e. mode shapes are real-valued and orthogonal with respect to the damping matrix [33]), and assuming a fixed condition at the base was employed. Since the model is elastic, its dynamic properties remain constant in time, that is, we use a time-invariant system identification. Furthermore, since the model is assumed to have a classical damping, the system of equations of motions can be decoupled and the predicted structural response was computed using modal superposition:

$$\hat{\ddot{u}}_j(t) = \sum_{n=1}^{N_m} \Gamma_n \phi_{nj} \ddot{D}_n(t) \tag{2}$$

where $\hat{\ddot{u}}_j(t)$ is the predicted relative acceleration at location j at time t; Γ_n is the modal participation factor of the $n-th$ mode, ϕ_{nj} is the mode shape of the $n-th$ mode evaluated at location j; N_m is the number of modes considered in the analysis, and $\ddot{D}_n(t)$ is the response of a single-degree-of-freedom system of unit mass, period T_n, and damping ratio ξ_n, when subjected to the ground motion acceleration at the base $\ddot{u}_g(t)$.

The reason for using this model is that currently it is the most common mathematical model employed in engineering practice for the seismic analysis buildings. Therefore, the identification results correspond directly to the modal damping ratios that a structural engineer should use in order to reproduce, as best as possible, the measured structural response when using the ground motion recorded at the base as input. If only N_m modes are considered in the structural model, and if the structure is assumed to be at rest at $t = 0$, then the parameters to identify are given by:

$$\theta = \left(\begin{Bmatrix} T_1 \\ \vdots \\ T_{N_m} \end{Bmatrix}; \begin{Bmatrix} \xi_1 \\ \vdots \\ \xi_{N_m} \end{Bmatrix}; \begin{bmatrix} \Gamma_1\phi_{11} & \cdots & \Gamma_{N_m}\phi_{N_m 1} \\ \vdots & \ddots & \vdots \\ \Gamma_1\phi_{1N_{sen}} & \cdots & \Gamma_{N_m}\phi_{N_m N_{sen}} \end{bmatrix} \right) \tag{3}$$

where T_n and ξ_n are the period and damping ratio of the $n-th$ mode of vibration, respectively; $\Gamma_n\phi_{nj}$ is the product of the modal participation factor and the mode shape of the $n-th$ mode evaluated at the location of the $j-th$ sensor, respectively. For more details on the optimization problem, such as initial set of parameters, or optimization constraints, the reader is referred to [8].

4. Building LA-32: example of an actual building subjected to several earthquakes

This section describes a 32-story residential building located in downtown Los Angeles that will be used as an example in the subsequent sections. The building is monitored by the California Strong Motions Instrumentation Program (CSMIP station No. 24288) and was selected because it has been shaken by multiple earthquakes, but also because its seismic response has an important contribution from higher modes. Therefore, it provides an opportunity to assess the reliability of damping ratios of higher modes inferred from different earthquakes. The building base dimensions are 38 m by 27 m, and has a total height of 103 m. The vertical carrying load system is composed of lightweight concrete slabs, supported by steel beams and columns. The lateral load resistant system consists of steel moment resistant frames located in the perimeter of the building. Although the building was designed in 1967, its current digital instrumentation system was installed in 2005. The system comprises 16 accelerometers at 5 different levels in the building, and has recorded 8 different earthquakes. Fig. 2 shows schematics of the building and the location of the different sensors. Due to space limitations, only the results for the EW_{ref} direction are discussed here. Table 4 shows the year, magnitude, distance to epicenter, and peak ground acceleration in the EW_{ref} direction of the different earthquakes recorded by this station.

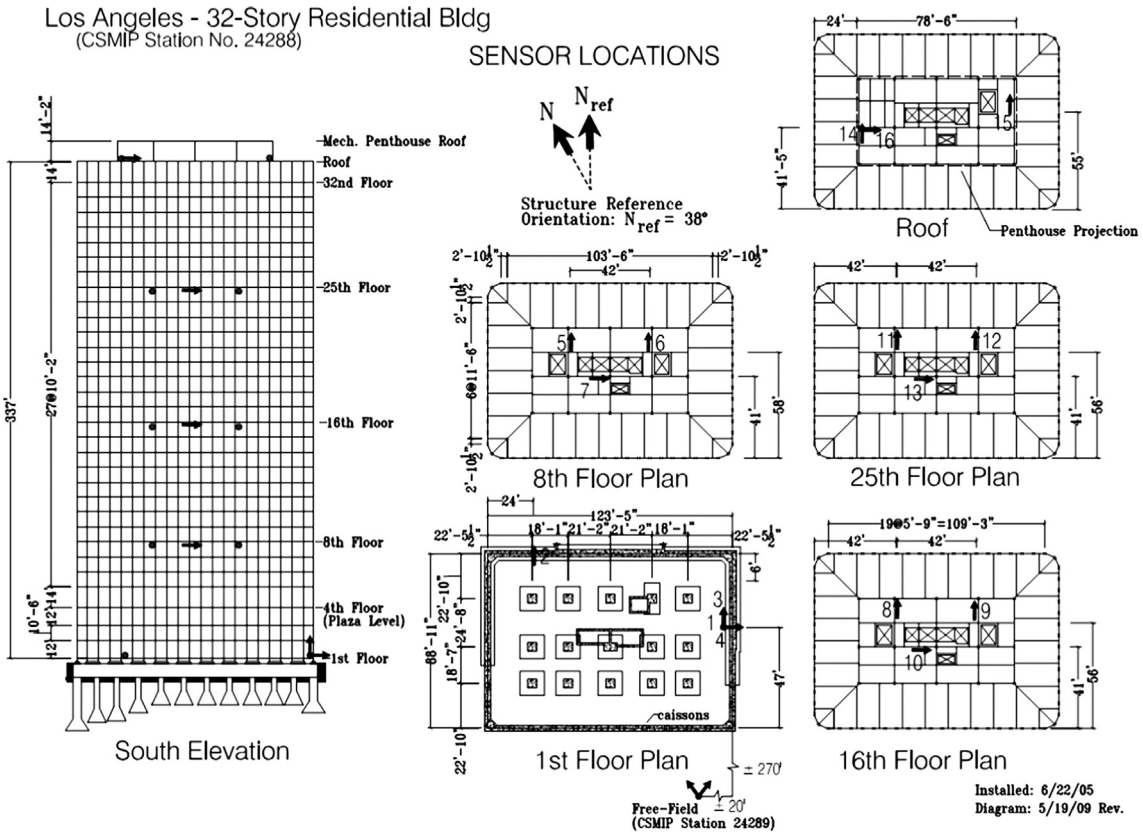

Fig. 2. Building schematics and sensor locations for LA-32 (after [34]).

Table 4
Recorded earthquakes for building LA-32-EW.

Earthquake	Year	Mw	Dist. to epicenter (km)	PGA (g)
Borrego Springs	2010	5.4	178.0	0.006
Calexico	2010	7.2	340.9	0.007
Chino Hills	2008	5.4	46.4	0.064
Encino	2014	4.4	23.3	0.008
Inglewood	2009	4.7	15.7	0.016
LA Airport	2012	3.7	17.6	0.007
La Habra	2014	5.1	33.8	0.013
Whittier Narrows	2010	4.4	17.8	0.033

5. Reliability metrics and screening tests

To be able to identify any parameter of the structural model, such as a modal damping ratio, then the parameter has to have a noticeable influence in the measured structural response. In other words, it is not possible to reliably estimate a parameter related to an aspect of the dynamic response that is not clearly observable. Therefore, the reliability of the identified damping ratio of, say, the $n-th$ mode, will depend on the level of contribution of the $n-th$ mode to the total structural response. Damping ratios of modes that contribute significantly to the dynamic response of the structure will be easier to identify than those from modes that contribute less to the total response. More importantly, understanding which modes are primarily participating in the structural response allows to question the reliability of the identified parameters of the modes that are not. A system identification method will yield parameters of as many modes as specified by the user, that is, the parameters that minimize the objective function, but some of the identified parameters may not be reliable as they may not correspond to those in the structure. For example, if the seismic response of a given building is primarily governed by the first 3 modes but the structural model employed in the identification considered 10 modes, the damping ratios beyond the third mode may not be reliable.

This investigation proposes 3 metrics to measure the reliability of damping ratios inferred from the seismic response of buildings. These metrics evaluate 3 different aspects that determine how much a mode is participating in the structural response. The first metric, namely the Dynamic Amplification Factors, measures the capacity of the recorded ground motion to excite the first two modes of the building. The second metric, called the Arias Modal Contribution, measures the relative contribution of the modes included in the structural model to the total structural response. Finally, the third metric, Reliability Intervals, measures the sensitivity of the response to changes in modal damping ratio, providing an interval of damping ratios that is likely to bracket the true damping ratio of the building.

Once these metrics are computed for all the identified modal damping ratios, they can be compared to threshold values than can be used to establish screening tests. If all the metrics are within acceptable values, and therefore pass all three screening tests, then the damping value is deemed to be reliable. The subsequent sections explain the different reliability metrics and their corresponding limiting values to be used as screening tests. Please note that these thresholds are arbitrary. They were defined after the inspection of numerous damping ratios inferred from multiple buildings and earthquakes, but other limiting values could be used. As with other limiting criteria, there is a tradeoff between using a relaxed criteria that keeps more data but less reliable, and a stricter threshold that yield less but more reliable results. The limits proposed in this investigation were defined to have stricter limiting values, as it was decided that it was better to reject modal damping ratios that might be correct than to accept damping ratios that are incorrect.

There are many other factors that are known to affect the variability of the identified damping ratios, such as the parameters involved in the digital processing of the signals, the time window employed to perform the identification, or errors inherent to the system identification

technique employed. The influence of these factors can be found on several other investigations on the subject (e.g. [13,35–37]). The metrics proposed herein aim to evaluate the reliability of damping ratios from the perspective of how much a mode is participating in the structural response, all other variables being equal.

5.1. Dynamic amplification factors

It can occur that an earthquake is not capable of significantly exciting the first, or sometimes even the second mode of a building, but it can still excite its higher modes enough to infer their damping ratios. For example, for buildings on rock or firm soils, there are typically much larger spectral ordinates for periods less than 1 s than those larger than 1 s. Therefore, the dynamic response of tall buildings to this kind of ground motions will have a significant contribution of higher modes, but a very small participation of the first (and sometimes the second) mode. Thus, the parameters inferred for the first mode may not be reliable.

The Dynamic Amplification Factors, R_n, are a reliability metric that are particularly effective at quantifying the level of excitation of the first two modes. It provides a measure of the amplification of 1%-damped floor spectral acceleration ordinates averaged in the vicinity of the modal period in question for the motion recorded at the roof with respect to those of the motion recorded at the base of the building as follows:

$$R_n = \frac{\bar{S}_{ar}(T_n)}{\bar{S}_{ab}(T_n)} \tag{4}$$

where $\bar{S}_{ar}(T_n)$ and $\bar{S}_{ab}(T_n)$ are the average of the 1%-damped floor spectral acceleration ordinates of the motions recorded at the roof and at the base of building, respectively, within the period range defined by $[0.9T_n, 1.1T_n]$, plus 0.01 g. The spectral acceleration ordinates are computed using a period interval $\Delta T = 0.01$ s. The purpose of the increment of the spectral ordinates in 0.01 g is to avoid excessive spectral ratios when values are close to zero in the denominator. Although this metric could be applied to any other mode of vibration, it was found that it was particularly useful in discriminating reliable modal damping ratios of the first and second mode. For higher modes, other metrics, explained in the next sections were shown to be better. After careful evaluation of various alternatives, the cut-off criteria for R_n was established to be:

$$R_1 \geq 2.2 \tag{5}$$

$$R_2 \geq 1.6 \tag{6}$$

Fig. 3 shows the roof and base 1%-damped response spectra for all the earthquakes recorded by building LA-32 in its EW reference direction. The figure indicates the computed R_n values for each earthquake. Also, the period windows that define R_1 and R_2 have been delimited with vertical dashed lines, and the roof and base spectra within these windows have been colored to highlight the amplification of the spectral ordinates for the first two modes. From the figure, it can be seen that the ground motions that caused a dynamic amplification factor for the first mode larger or equal than 2.2 correspond to the 2010 Borrego Springs, 2010 Calexico, 2008 Chino Hills, and 2014 La Habra earthquakes. The average fundamental period identified under these earthquakes is 2.90 s. Under most earthquakes, the period window corresponding to the first mode is centered roughly at 2.90 s, except for 2012 LA Airport and 2010 Whittier Narrows earthquakes, in which the identified periods for the first mode were 1.82 s and 2.32 s, respectively, and the identified damping ratio was 30% in both cases. Note that 30% corresponds to the upper bound of the identification process, meaning that the optimization algorithm will not look for damping values greater than 30%. Evidently, the first mode is barely getting excited under these two ground motions and therefore the periods and damping ratios obtained are not correct. The values of R_1 for these two earthquakes are 1.01 and 1.10, respectively, which are well below the threshold of 2.2, indicating that the damping ratios obtained for the first mode are not reliable.

5.2. Arias modal contribution

The seismic response of a building can in most cases be correctly reproduced by considering only a small number of modes (e.g., [32,38]). If the structural model employed in the system identification problem shown in Eq. (1) considers modes that have a negligible contribution to the seismic response, then the results obtained for these modes may not be reliable. Thus, measuring the relative contribution of the different modes to the computed seismic response at the different instrumented levels in the building, and establishing a minimum contribution as a cut-off criteria can provide a way to detect damping ratios that may not be reliable. To this purpose, the Arias modal contribution factor, MC_n of a given mode (say, the $n-th$ mode) was defined as the relative contribution, measured in terms of the Arias intensity of the signal, of the $n-th$ modal response with respect to that calculated with N_m modes. Mathematically, MC_n is calculated as follows:

$$MC_n = \frac{\sum_{j=1}^{N_{sen}} \sum_{k=1}^{\tau} [\ddot{\hat{u}}_{nj}(k\Delta t)]^2}{\sum_{i=1}^{N_m} \sum_{j=1}^{N_{sen}} \sum_{k=1}^{\tau} [\ddot{\hat{u}}_{ij}(k\Delta t)]^2} \tag{7}$$

where MC_n is the Arias modal contribution of the $n-th$ mode; $\ddot{\hat{u}}_{ij}$ is the relative acceleration computed for the $i-th$ mode of vibration at floor j; Δt is the digitization time step of the record; N_m is the total number of modes considered in the structural model; N_{sen} is the number of sensors above ground level; and τ is the number of data points in the record. As noted by Chopra [39] sd, modal participation factors, by themselves do not provide information about how much a particular mode is contributing to the total response. Please note that unlike, the modal contribution factors proposed by Chopra, that correctly account for the factors in the structure that contribute to the total response, the Arias modal contribution used here account for factors both in the structure and in the ground motion that make the contribution of each modal response to the response parameters being measured.

As an example, Fig. 4 shows the deaggregation of the different modal components of the computed relative acceleration at the roof of building LA-32 – described in Section 4 – when subjected to the EW component of the 2008 Chino Hills earthquake. For this case, it can be seen that at the roof the third mode provides the highest relative contribution to the response, followed by the second, fundamental, and fourth modes. The contribution of the fifth mode is considerably smaller than the rest of the modes, but it is slightly larger than 5% so this mode would be taken into account. The sixth mode, however, contributes less than 5% so the inferred damping ratio for this mode would be discarded in this case since their contribution to the total response is relatively small. Please note that the Arias modal contributions are computed considering all the sensors in the building, not just the roof, but in the figure only the roof response is displayed. Even when the fifth mode may not be seem to be contributing to the response at the roof, it may be contributing to the response in other locations due to the distribution of the sensors along the height of the building. Also, the modal contributions will be affected by the intensity and frequency content of the earthquake so the different modal contributions will change from earthquake to earthquake.

5.3. Sensitivity of the objective function

5.3.1. Reliability intervals

In the previous sections it has been shown that the variability in the identified damping ratios is significantly higher than the variability in the identified periods. In order to understand why this occurs, it is necessary to analyze the sensitivity of the objective function to small variations in periods and damping ratios. Fig. 5 shows the variation of the objective function with changes in the fundamental period and with

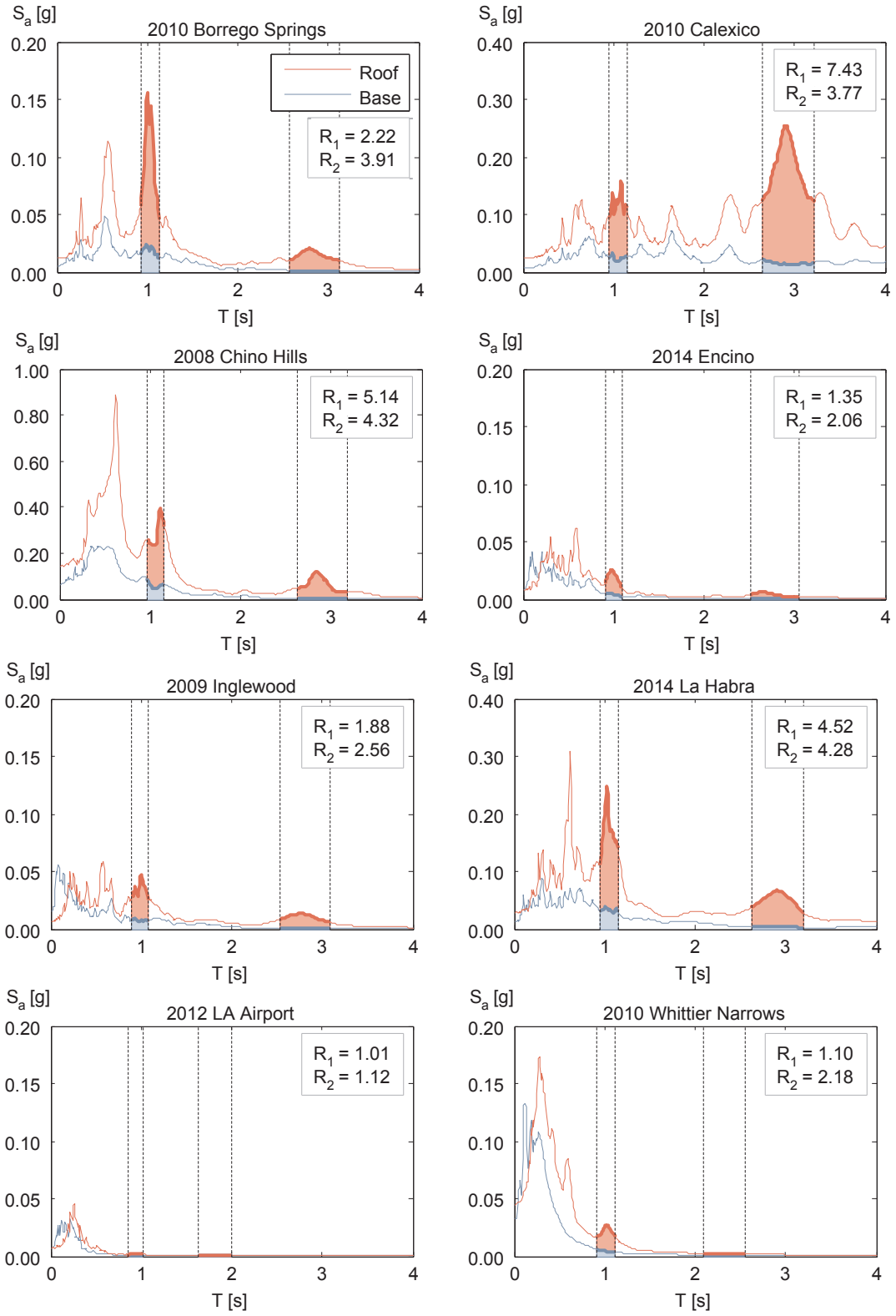

Fig. 3. Roof and ground acceleration response spectrum (ξ = 1%) for the E-W direction of building LA-32 for all earthquakes recorded by this station.

changes in the damping ratio of the first mode of building LA-32 under the 2010 Borrego Springs earthquake in the EW direction while keeping constant the rest of the parameters in the model. For the first mode, the identified period is $T_1 = 2.85$ s and the identified damping ratio is $\xi_1 = 2.0\%$. These parameters minimize J, whose minimum can be seen in the surface shown in Fig. 5. Fig. 6 shows the contour curves of equal value of J near the minimum of the function, spaced at increments of 1% of the minimum value of J. It can be seen that, near the minimum, the contours are approximately shaped as elongated ellipses, with their major axis oriented in the direction of damping. The contour level that is 1% higher than the minimum value of the function delimits intervals in damping ratios and periods, which are shown in segmented lines in

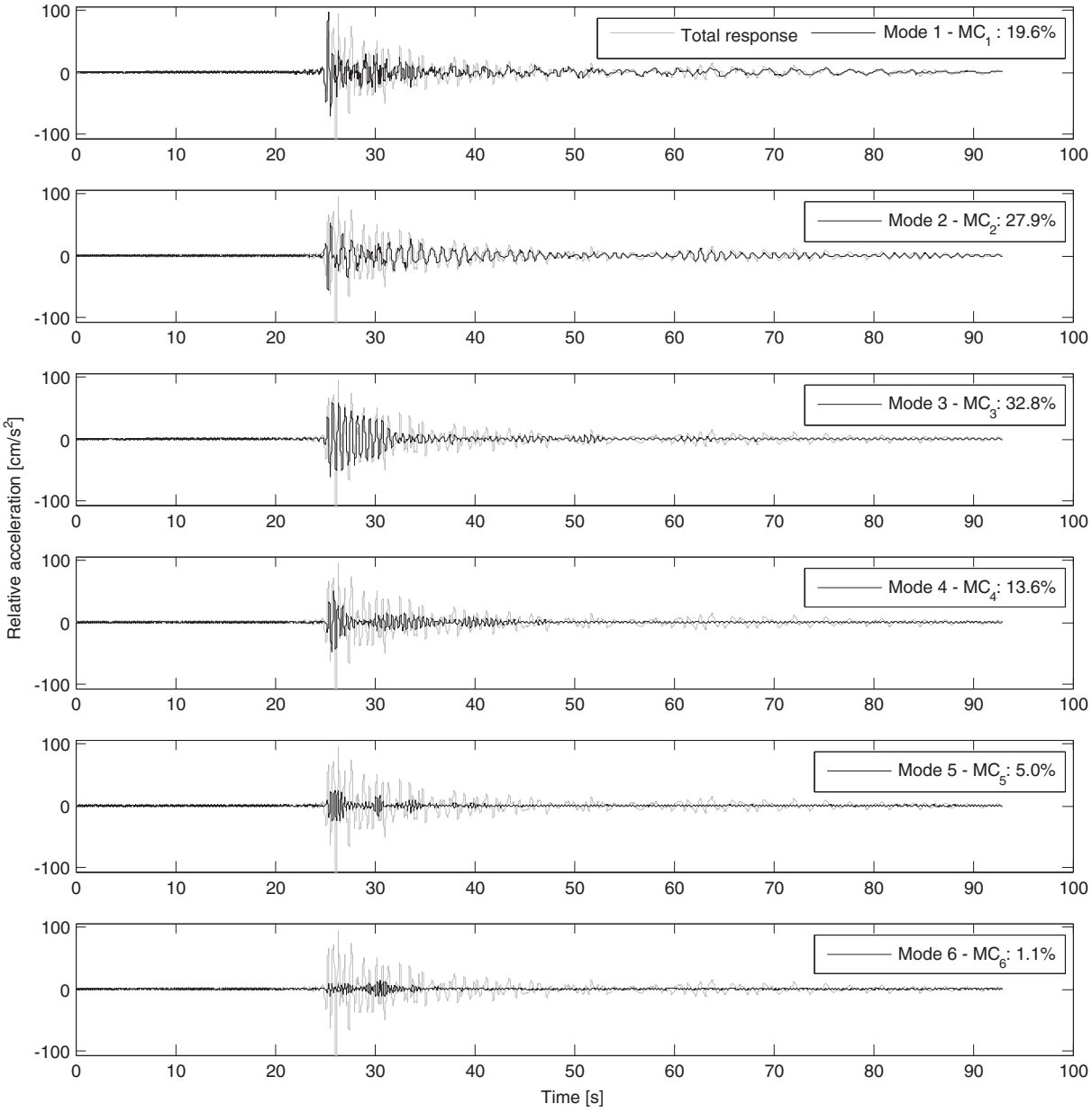

Fig. 4. Deaggregation of the contribution of the first six modes to the relative acceleration at the roof, for the EW direction of building LA-32 subjected the 2008 Chino Hills Earthquake.

Fig. 6. Any variation in damping ratio or period beyond outside this contour will cause an increment greater than 1% in the value of the objective function. In the figure, it can be seen that the range of periods within this contour curve is approximately from 2.81 to 2.89 s, and that the difference between these two periods is just 0.08 s, indicating that the correct value of the fundamental period is within 0.04 s of 2.85 s, in other words, within an error of ±1.4%. On the other hand, the range of damping ratios within the 1% contour curve is approximately from 1.1% to 3.4%, and the width of this range is about 2.3%, indicating that the correct value of the damping ratio is within −0.9% and +1.4% of 2.0%, which corresponds to an error of −45% and +70%. In other words, incrementing the value of the fundamental period by 0.04 s, an increment of just 1.4%, produces the same variation in the objective function as when increasing the damping ratio of the first mode from 2.0% to 3.4% (an increment of 70%). Therefore, for the same effect on the objective function, an error in the identification of the damping ratio can be significantly higher than that of the fundamental period.

The larger sensitivity of the objective function defined by Eq. (1) to changes in modal periods/frequencies compared to that produced by changes in modal damping ratios, as illustrated in Fig. 6, is partly inherent in the selection of this objective function. If a given trial of a modal period is inaccurate (i.e., it is shorter or longer than the optimum parameter), and it is used in combination with the optimal/correct modal damping ratio, then the computed relative acceleration $\hat{\ddot{u}}_j(t)$ will be out of phase with respect to the measured relative acceleration $\ddot{u}_j(t)$ not only throughout the whole history of the records but also in all sensors, leading to a large increment in the objective function. Meanwhile, for lightly damped structures, when using an inaccurate estimate of a modal damping ratio combined with an accurate estimate of a modal period the computed and measured responses will be in phase but with the incorrect amplitude. This will lead to a much smaller increment in the objective function than the one produced by an inaccurate modal period. This explains why the variability in damping ratios inferred from different earthquakes can be significantly higher than the variability in the inferred periods. The width of these intervals can be used to measure the reliability of the inferred damping ratios

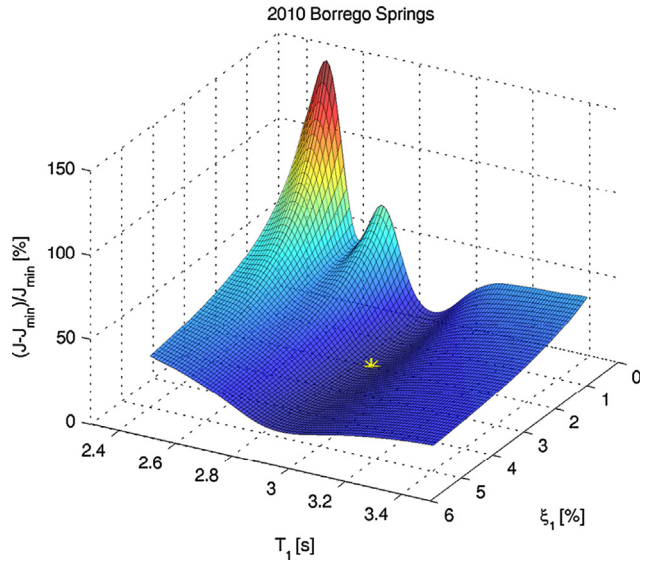

Fig. 5. Normalized objective function as a function of the modal damping ratio and modal period of the fundamental mode for the LA-32 building under the 2010 Borrego Spring earthquake, in the EW direction. The star indicates the minimum value of the objective function.

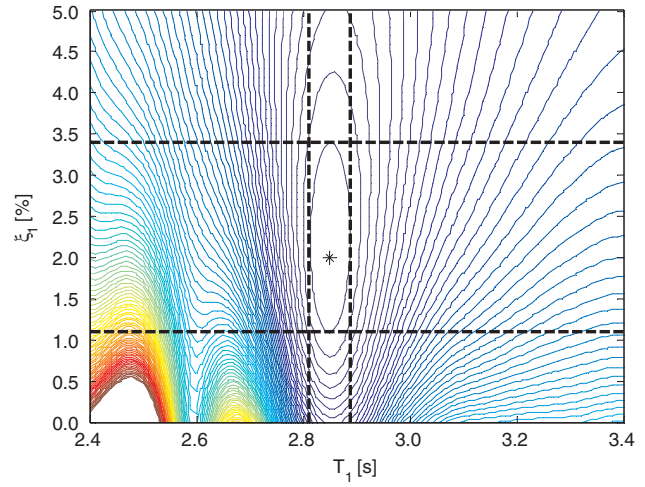

Fig. 6. Contour levels near the minimum value of the normalized objective function for the damping ratio and period of the first mode for the LA-32 building under the 2010 Borrego Spring earthquake, in the EW direction. The star indicates the location of the minimum value of the objective function.

since it is a measure of the slope of the objective function produced by changes in the $i-th$ modal damping ratio. More formally, this width is a measure of the partial derivative of the objective function with respect to the modal damping ratio in the vicinity of the modal damping ratio producing the minimum in the objective function.

Table 5 lists the identified damping ratios, reliability interval limits, and interval lengths for the first mode obtained for all the earthquakes recorded in building LA-32. Fig. 7 shows the variation of the objective function with changes in the damping ratio of the first mode in the EW direction while keeping all the other parameters constant and equal to their optimal values. It can be seen that the sensitivity of the objective function to changes in the damping ratio of the first mode, as measured by the reliability intervals, changes considerably from earthquake to earthquake. The smallest reliability interval was obtained under the 2010 Calexico earthquake ($\xi_1 = 2.0\%$), indicating that the damping ratio of the first mode, under this specific ground motion, has the largest effect in the objective function and therefore is the most reliable

Table 5
Identified first mode damping ratios, reliability interval limits, and interval length for all the earthquakes recorded in building LA-32-EW.

Earthquake	ξ_1 [%]	ξ_{Lower} [%]	ξ_{Upper} [%]	Interval length [%]
2010 Borrego Springs	2.0	1.1	3.3	2.2
2010 Calexico	2.0	1.9	2.0	0.1
2008 Chino Hills	2.4	1.9	3.0	1.1
2014 Encino	3.5	0.8	14.6	13.8
2009 Inglewood	2.3	1.3	4.2	2.9
2012 LA Airport	30.0*	19.7	Capped	–
2014 La Habra	2.0	1.7	2.5	0.8
2010 Whittier Narrows	30.0*	10.3	Capped	–

* 30% was set as an upper bound, all damping ratios larger than 30% are considered to be unreliable.

estimation of the damping ratio of the structure. From the figure, there is an evident correlation between the length of the reliability interval and the consistency in the obtained damping ratios. For example, damping ratios obtained under earthquakes with an interval length smaller than 3%, in ascending order are: 2.0% damping for the 2010 Calexico, 2.0% for the 2014 La Habra event, 2.4% for the 2008 Chino Hills event, 2.0% for the 2010 Borrego Springs event, and 2.3% damping for the 2009 Inglewood event. From these results, it can be concluded that the damping ratio of the structure is between 2.0% and 2.4%. The opposite is true for those earthquakes with wide reliability intervals: 3.5% (2014 Encino), and 30% (2012 LA Airport and 2010 Whittier Narrows), where the objective function is not very sensitive to changes in the damping ratio of the first mode and therefore leading to less credible results with a higher dispersion. The reliability intervals are related to both the level excitation and to the relative contribution of the mode being analyzed. In general, modes with low *MC* values will tend to have wide reliability intervals, while modes with high *R* values will tend to have narrower intervals.

5.3.2. Enhanced reliability intervals

The previous section described a method to quantify the reliability of the inferred damping ratios by measuring the sensitivity of the objective function to small variations in the modal damping ratios. However, in most cases the objective function, as defined in Eq. (1), will be more sensitive to parameters that govern the fundamental mode than those that control higher modes simply because the fundamental mode typically has a larger contribution to the response. Therefore, it is necessary to also have a parameter that is more sensitive to the specific response of the mode being analyzed, rather than to the sum of all modes.

To obtain reliability intervals that are more sensitive to the response of higher modes, it is necessary to redefine the objective function in order to make it more sensitive to small variations of modal damping ratios in higher modes. A way to achieve this is to perform an additional system identification with a single parameter to be identified, corresponding to the damping ratio of the mode whose reliability is being measured. All the other parameters – periods, damping ratios and mode shapes – are kept constant and equal to those initially identified. Since there is only one variable involved in this additional system identification scheme only one output sensor location is required. The recorded response at the roof is selected because it always contains information about higher modes, avoiding possible node locations, and because practically all buildings have sensors located at the roof. To isolate the contribution of the mode being analyzed, the response at the roof was filtered using a bandpass filter that removes the frequency content of the signal that is not within the vicinity of the modal frequency identified for this particular mode. For the same reason, the ground motion record was also filtered within the same frequency range. Using the filtered ground motion as input, an optimization routine was employed to find the damping ratio that would make the system best reproduce

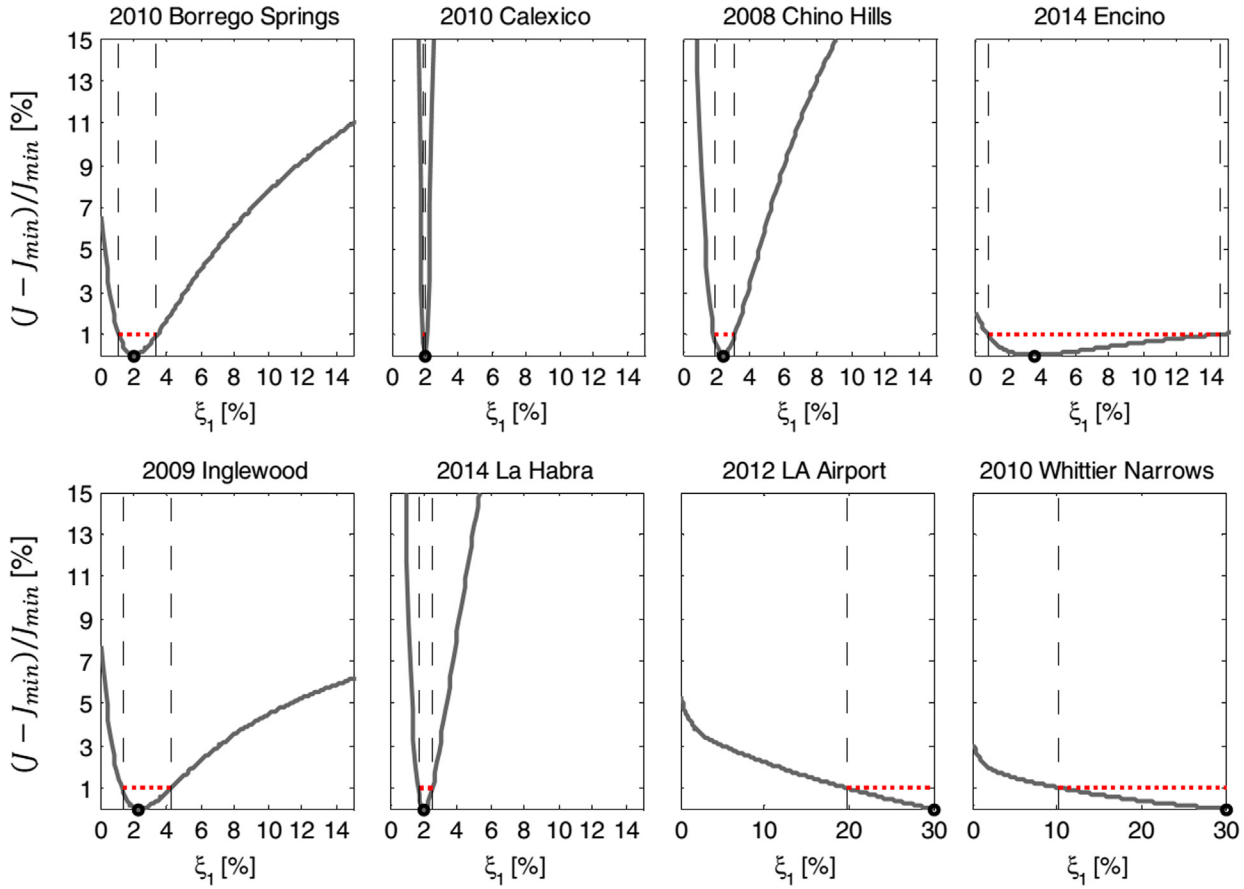

Fig. 7. Variation of the normalized objective function J with changes in the damping ratio of the first mode for building LA-32-EW, during all the earthquakes recorded by this station.

the filtered response at the roof. Please note that this equivalent to finding the damping ratio of an SDOF system with period T_n subjected to the filtered ground motion, and having its response amplified by $\Gamma_n\phi_{nroof}$, that would best reproduce the filtered recorded response at the roof, where T_n and $\Gamma_n\phi_{nroof}$ correspond to the identified period and effective mode shape at the roof for the mode being analyzed. The objective function of this simple identification process was plotted against the modal damping ratio, and a new reliability interval was computed. Since there is only one variable involved, the objective function is now very sensitive to changes in the damping ratio. For this reason, the boundaries for this new intervals were set as those damping values that cause a variation of less than 50% of this new objective function, instead of the previous 1%. This interval is defined as the enhanced reliability interval (ERI) of the inferred damping ratio. Note that the aforementioned procedure was only used to quantify the reliability of the damping ratios identified originally. A detailed, step-by-step guide on how to compute the enhanced reliability intervals is detailed below.

5.3.3. Steps to compute the enhanced reliability intervals

i. **Perform the system identification**

The identification was done using the parametric minimization method described in Section 3. Then for each of the identified modal damping ratios, steps 2 to 6 were followed.

ii. **Define the bandpass filter's corner frequencies**

The lower and upper frequencies (f_L and f_U, respectively) of the bandpass filter were defined as:

$$f_L = 0.5\cdot(f_{n-1} + f_n) \tag{8}$$

$$f_U = 0.5\cdot(f_n + f_{n+1}) \tag{9}$$

$$f_{L_1} = f_1/2 \tag{10}$$

$$f_{U_{Nm}} = 2f_{N_m} \tag{11}$$

where f_n is the identified frequency of the $n-th$ mode ($f_n = 1/T_n$), and f_{L_1} and $f_{U_{Nm}}$ are the lower and upper cutoff frequencies for the first and last modes being considered, respectively.

iii. **Filter the recorded ground motion and the recorded acceleration at the roof**

A Butterworth digital filter of order 3, with passband $f_L < f < f_U$ was applied to the ground and roof acceleration records. These filtered records at ground (g) and roof (R) levels are further referred as $\ddot{u}_g^F$ and $\ddot{u}_R^F$, respectively.

iv. **Compute the response of an equivalent SDOF**

The response of an equivalent single-degree-of-freedom system with period T_n and damping ratio $\hat{\xi}_n$ subjected to the filtered ground motion acceleration record was computed. The response was the amplified by the identified effective mode shape $\Gamma_n\phi_{nroof}$ of the mode being analyzed. This response is denoted as $\ddot{\hat{u}}_R^F$.

v. **Define and solve the secondary optimization problem**

The secondary optimization problem is defined by the following

objective function:

$$J_s = \sum_{k=1}^{\tau} [\ddot{u}_R^F(k\Delta t) - \hat{\ddot{u}}_R^F(k\Delta t)]^2 \quad (12)$$

where τ is the number of points in the records, and Δt is the time step. Given the small number of parameters involved, the solution to this problem is extremely simple to obtain, as it can be quickly solved by the following brute-force approach. To solve it, the damping ratio $\hat{\xi}_n$ of the SDOF system was varied over a wide range of values. For each value of $\hat{\xi}_n$ the objective function of the secondary optimization problem J_s was evaluated using Eq. (12). The optimal value of $\hat{\xi}_n$ was found as that minimizes the value of J_s.

vi. **Compute the enhanced reliability interval**

The values of J_s computed in step (v) were normalized by its minimum value J_s^{min}. The enhanced reliability intervals were then computed as the range of damping ratios that caused J_s to vary in less than 50% of its minimum value.

5.3.4. Maximum allowable enhanced reliability intervals

The enhanced reliability intervals (ERI) quantify the contribution of each mode to the structural response by measuring the sensitivity of the objective function to small variations of the modal damping ratios. In this screening test, a maximum length of the enhanced reliability interval was established to determine which damping ratios would be considered in further analyses. Since higher modes in most cases will have a smaller contribution to the total structural response, the sensitivity of the objective function to modal damping ratios will typically decrease with mode number. Consequently, the maximum allowed interval length was set as a function of the modal frequency. Since low-rise structures tend to have higher fundamental frequencies, the cutoff for the fundamental mode was set to be stricter than for higher modes. The maximum allowed ERI lengths are shown in Fig. 8. Please note that the length measures the difference between the damping ratios that cause an increment of 50% of the minimum value on the objective function of the secondary optimization problem J_s defined in Eq. (12), therefore the interval length has the same units than the damping ratio (i.e., non-dimensional or percentage). Only the damping ratios of modes having an enhanced reliability interval length smaller than the maximum allowed limits were considered in further analyses.

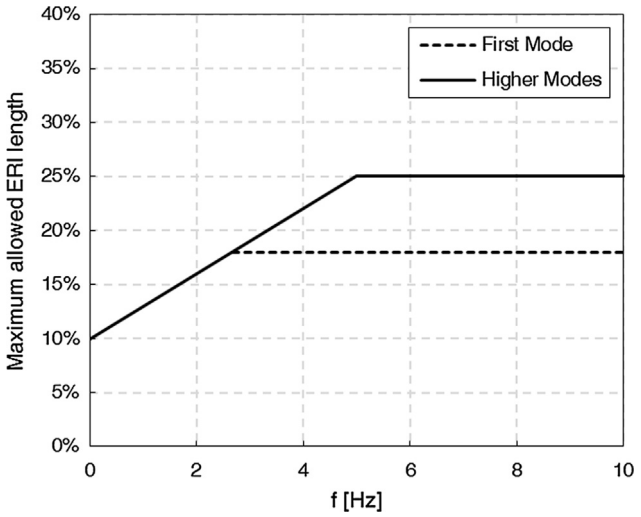

Fig. 8. Maximum allowable length of the enhanced reliability intervals.

6. Example

This section provides an example of how the different reliability screening tests are applied after the initial system identification results are obtained. For this example, the EW direction of building LA-32 – described in Section 4 – is used. The dynamic properties of the buildings were inferred using the parametric minimization method along with a planar model of the building. The results of the identification for all the different earthquakes can be seen in Fig. 9, which plots the identified modal damping ratios against their corresponding modal frequencies. The identified modal periods, frequencies, and damping ratios, as well as their corresponding amplification factors (R), Arias modal contribution ratios (MC), and enhanced reliability interval lengths (ERI), are listed on Table 6.

Fig. 9a shows the raw data obtained from the identification. It can be seen that there are clusters of data points, corresponding to the damping ratios at the different modal frequencies. At about 0.5 Hz, however, there are two points with damping ratios of 30%, which were obtained for the 2010 Whittier Narrows, and for the 2012 LA Airport earthquakes. As mentioned in Section 5.1, this damping value corresponds to the upper bound of the identification process, meaning that the optimization algorithm will not look for damping values greater than 30%. Obviously, these two values cannot correspond to the true value of the damping ratio of the fundamental mode, as they are most likely the byproduct of the low sensitivity of the objective function to variations in the damping ratio of the fundamental mode for those particular earthquakes because the fundamental mode is practically not excited and at the fundamental frequency the building experiences an almost rigid-body behavior. These two earthquakes are not capable of exciting the fundamental mode enough to infer a reliable damping value out of the records. Fig. 9b shows the same information as Fig. 9a, but in this case those data points that do not pass the amplification factor reliability tests are highlighted in blue. It can be seen that the two aforementioned outliers are correctly identified as not reliable and screened out by this reliability screening test. Moreover, the dynamic amplification factors screening test also filters out two more damping ratios from the fundamental mode and one from the second mode – this is better appreciated in Fig. 9c, where results are plotted at a reduced vertical scale – significantly reducing the variability in the results of the fundamental mode. Fig. 9c also highlights in red[1] those data points that do not pass the Arias modal contribution screening test. This screening test identifies all the results of all those modes contributing less than 5% of the total structural response. It can be seen that this screening test reduces the dispersion obtained for the fifth mode and eliminates almost all the data points obtained for the sixth mode, most of which visually appear strange. Fig. 9d highlights in magenta all those points that do not pass the enhanced reliability interval screening test. It can be seen that this test removes the reminder of points coming from the sixth mode, but one. Although not shown in the figure, this last test also rules out the aforementioned 30% damped points for the fundamental mode. Finally, only those points that have passed all the reliability screening tests are reported (Fig. 9e).

7. Summary and conclusions

This paper evaluated the reliability of modal damping ratios inferred from the measured seismic response of buildings using parametric system identification methods. It was shown that different authors often report different identified values for buildings being analyzed under the same earthquake, that is, using the same data but using different identification methods. These differences were significantly larger in the reported damping ratios than in the reported modal periods.

Three different metrics to assess the reliability of the results and to

[1] For interpretation of color in Fig. 9, the reader is referred to the web version of this article.

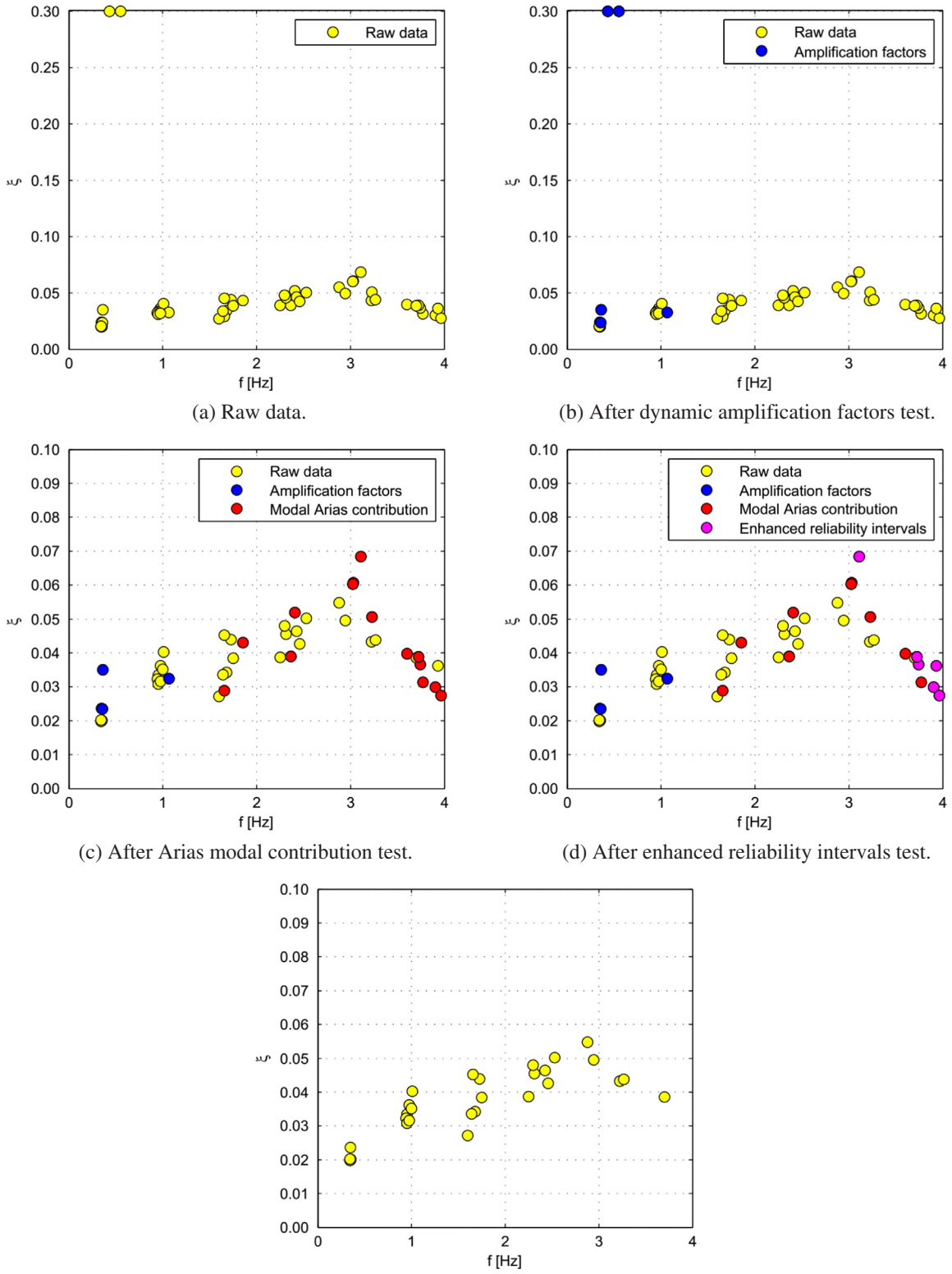

(a) Raw data.

(b) After dynamic amplification factors test.

(c) After Arias modal contribution test.

(d) After enhanced reliability intervals test.

(e) Final results after the application of all tests.

Fig. 9. Example of implementation of reliability screening tests on building LA-32-EW.

screen out those deemed not to be reliable were presented: The dynamic amplification factors, Arias modal contribution, and enhanced reliability intervals. The dynamic amplification factors provide a measure of the amplification of 1%-damped floor spectra acceleration ordinates averaged in the vicinity of the identified modal periods for the recorded response at the roof with respect to those of the motion recorded at the base of the building. This metric provides information if the earthquake provides enough excitation in the vicinity of a particular mode to generate a response of that mode that is strong enough to allow a reliable identification of the modal damping ratio. This metric can be used on any mode, but it was found that this particular effective for identifying damping ratios of the first and second modes of the

Table 6
Identified periods, damping ratios, and reliability metrics for LA-32 EW.

Earthquake	T [s]	f [Hz]	ξ	R	MC	ERI
Mode 1						
Borrego Springs 2010	2.85	0.35	2.0%	2.22	15.2%	2.0%
Calexico 2010	2.93	0.34	2.0%	7.43	74.7%	1.2%
Chino Hills 2008	2.90	0.34	2.4%	5.11	19.6%	1.0%
Encino 2014	2.78	0.36	3.5%	1.35	36.4%	3.2%
Inglewood 2009	2.81	0.36	2.4%	1.88	42.4%	1.2%
LA Airport 2012	1.82	0.55	30.0%	1.01	59.2%	23.8%
La Habra 2014	2.91	0.34	2.0%	4.52	22.8%	1.0%
Whittier Narrows 2010	2.32	0.43	30.0%	1.10	44.0%	39.0%
Mode 2						
Borrego Springs 2010	1.03	0.97	3.6%	3.91	63.7%	2.0%
Calexico 2010	1.05	0.95	3.3%	3.77	19.8%	2.2%
Chino Hills 2008	1.06	0.94	3.2%	4.32	27.9%	2.4%
Encino 2014	1.00	1.00	3.5%	2.06	20.7%	1.8%
Inglewood 2009	0.99	1.01	4.0%	2.56	29.6%	2.6%
LA Airport 2012	0.94	1.06	3.2%	1.12	11.2%	11.0%
La Habra 2014	1.05	0.95	3.1%	4.28	45.9%	1.4%
Whittier Narrows 2010	1.02	0.98	3.2%	2.18	13.4%	3.8%
Mode 3						
Borrego Springs 2010	0.60	1.68	3.4%	–	17.0%	1.8%
Calexico 2010	0.60	1.65	2.9%	–	4.1%	3.0%
Chino Hills 2008	0.62	1.60	2.7%	–	32.8%	0.8%
Encino 2014	0.58	1.73	4.4%	–	18.8%	3.2%
Inglewood 2009	0.57	1.75	3.8%	–	12.9%	1.8%
LA Airport 2012	0.54	1.85	4.3%	–	4.9%	6.6%
La Habra 2014	0.61	1.64	3.4%	–	21.3%	1.4%
Whittier Narrows 2010	0.60	1.65	4.5%	–	8.5%	3.6%
Mode 4						
Borrego Springs 2010	0.42	2.40	5.2%	–	2.4%	5.8%
Calexico 2010	0.42	2.36	3.9%	–	1.2%	3.2%
Chino Hills 2008	0.44	2.25	3.9%	–	13.6%	1.8%
Encino 2014	0.41	2.42	4.6%	–	10.4%	4.6%
Inglewood 2009	0.41	2.46	4.3%	–	7.7%	2.0%
LA Airport 2012	0.40	2.53	5.0%	–	7.7%	12.8%
La Habra 2014	0.43	2.31	4.6%	–	5.5%	2.6%
Whittier Narrows 2010	0.44	2.30	4.8%	–	15.5%	2.8%
Mode 5						
Borrego Springs 2010	0.32	3.11	6.8%	–	0.6%	37.6%
Calexico 2010	0.33	3.03	6.1%	–	0.2%	14.0%
Chino Hills 2008	0.35	2.88	5.5%	–	5.0%	5.0%
Encino 2014	0.31	3.22	4.3%	–	10.8%	2.8%
Inglewood 2009	0.31	3.23	5.1%	–	4.3%	5.4%
LA Airport 2012	0.31	3.26	4.4%	–	8.4%	3.0%
La Habra 2014	0.33	3.02	6.0%	–	3.3%	5.8%
Whittier Narrows 2010	0.34	2.95	5.0%	–	11.6%	3.8%
Mode 6						
Borrego Springs 2010	0.27	3.77	3.1%	–	1.1%	9.2%
Calexico 2010	0.27	3.74	3.7%	–	0.1%	49.2%
Chino Hills 2008	0.28	3.60	4.0%	–	1.1%	9.8%
Encino 2014	0.26	3.91	3.0%	–	2.9%	49.4%
Inglewood 2009	0.25	3.96	2.7%	–	3.2%	49.0%
LA Airport 2012	0.25	3.93	3.6%	–	8.5%	48.4%
La Habra 2014	0.27	3.72	3.9%	–	1.2%	48.2%
Whittier Narrows 2010	0.27	3.70	3.9%	–	6.9%	12.8%

structure that may not be reliable in situations when they are not sufficiently excited by the earthquake. The Arias modal contribution ratio uses the Arias intensity of a modal response to measure the relative contribution of each mode to the total response. This metric was found particularly useful in identifying higher modes that are not contributing significantly to the total response at the location of the sensors and therefore, damping ratios identified for these modes may not be reliable. Finally, the reliability intervals measure the sensitivity of the objective function to small variations in the damping ratio. It was found that the objective function can be significantly more sensitive to variations in damping ratios than to variations in the modal periods, which explains the larger variability in the results for damping with respect to that obtained in periods. A method to obtain reliability intervals that are more sensitive to the response of higher modes, called enhanced reliability intervals, was also presented. Reliability screening tests were developed based on these three metrics. Using a 32-story building as an example, it was shown that these tests are capable of detecting and screening out unreliable results in order to keep those deemed reliable.

The three metrics can be applied to the results of any system identification technique capable of determining modal periods, damping ratios, mode shapes, and modal participation factors, provided that the input to the system (ground motion at the base of the building) has been recorded. Please note that although the Enhanced Reliability Intervals (ERI) metric is based on the "Reliability Intervals" method – which requires measuring the sensitivity of the objective function to changes in damping ratios and therefore is applicable only to Prediction Error Methods (e.g., Modal Minimization [10], ARX [40], ARMAX [40], Discrete-Time Filters [12], etc.) – ERI are calculated based on a secondary SDOF system and therefore can be applied to the results of any system identification method that satisfies the aforementioned requirements.

Acknowledgements

The authors would like to acknowledge CONICYT – Becas Chile, the Blume Earthquake Engineering Center at Stanford University, and the Shaw Family Fund for the financial aid to the first author for conducting doctoral studies at Stanford under the supervision of the second author. Ground and structural motions used in this investigation were obtained from the California Strong Motion Instrumentation Program of the California Geological Survey and from the United States Geological Survey. Efforts to install, operate, and maintain seismic instrumentation in buildings as well as to process and disseminate earthquake records by these organizations are gratefully acknowledged.

References

[1] Kijewski-Correa TL. Full-scale measurements and system identification: a time-frequency perspective. University of Notre Dame; 2003.
[2] Strutt JW. The theory of sound, vol. 1, 2nd ed. London and New York: Macmillan and Co.; 1894.
[3] Jacobsen LS. Steady force vibration as influenced by damping. Trans Am Soc Mech Eng 1930;52:169–81.
[4] Beck JL. Determining models of structures from earthquake records. Report No. EERL 78–01. California Institute of Technology; 1978.
[5] McVerry G. Frequency domain identification of structural models from earthquake records. Report No. EERL 79–02. California Institute of Technology; 1979.
[6] Safak E, Celebi M. Seismic response of Transamerica building. II: system identification. J Struct Eng 1991;117:2405–25.
[7] Cruz C, Miranda E. Evaluation of the Rayleigh damping model for buildings. Eng Struct 2017;138:324–36. https://doi.org/10.1016/j.engstruct.2017.02.001.
[8] Cruz C, Miranda E. Evaluation of damping ratios for the seismic analysis of tall buildings. J Struct Eng 2016;143:04016144. https://doi.org/10.1061/(ASCE)ST.1943-541X.0001628.
[9] Beck R. Fundamental problems in the application of structural identification procedures to damage detection. Report No. EERL. California Institute of Technology; 1991. p. 91–103.
[10] Beck JL, Jennings PC. Structural identification using linear models and earthquake records. Earthq Eng Struct Dyn 1980;8:145–60.
[11] McVerry GH. Structural identification in the frequency domain from earthquake records. Earthq Eng Struct Dyn 1980;8:161–80. https://doi.org/10.1002/eqe.4290080206.
[12] Safak E. Identification of linear structures using discrete-time filters. J Struct Eng 1991;117:3064–85.
[13] Ghanem R, Shinozuka M. Structural-system identification. I: theory. J Eng Mech 1995;121:255–64.
[14] Di Ruscio D. Combined deterministic and stochastic system identification and realization: DSR - A subspace approach based on observations. Model Identif Control 1996;17:193–230.
[15] Safak E, Celebi M. Recorded seismic response of Pacific Park Plaza. II: system identification. J Struct Eng 1992;118:1566–89.
[16] Celebi M. Highlights of Loma Prieta responses for four tall buildings. Tenth World Conf Earthq Eng. Rotterdam: Balkema; 1992. p. 4039–44.
[17] Goel RK, Chopra AK. Vibration properties of buildings determined from recorded earthquake motions. Earthquake Engineering Research Center, Report No. EERC-97. Berkeley: University of California; 1997.
[18] Bernal D, Dohler M, Kojidi SM, Kwan K, Liu Y. First mode damping ratios for buildings. Earthq Spectra 2015;31:367–81. https://doi.org/10.1193/

101812EQS311M.
[19] Pridham BA, Wilson JC. Identification of base-excited structures using output-only parameter estimation. Earthq Eng Struct Dyn 2004;33:133–55. https://doi.org/10.1002/eqe.343.
[20] Ghahari F, Abazarsa F, Ghannad MA, Taciroglu E. Response-only modal identification of structures using strong motion data. Earthq Eng Struct Dyn 2013;42:1221–42. https://doi.org/10.1002/eqe.2268.
[21] Ghahari F, Taciroglu E. Identification of damping ratios for soil-structure systems from seismic response signals. In: 11th US Natl Conf Earthq Eng, Los Angeles, CA; 2018.
[22] Lignos DG, Miranda E. Estimation of base motion in instrumented steel buildings using output-only system identification. Earthq Eng Struct Dyn 2014;43:547–63. https://doi.org/10.1002/eqe.2359.
[23] Pioldi F, Ferrari R, Rizzi E. Seismic FDD modal identification and monitoring of building properties from real strong-motion structural response signals. Struct Control Heal Monit 2017;24:1–20. https://doi.org/10.1002/stc.1982.
[24] Pioldi F, Rizzi E. A Full Dynamic Compound Inverse Method for output-only element-level system identification and input estimation from earthquake response signals. Comput Mech 2016;58:307–27. https://doi.org/10.1007/s00466-016-1292-0.
[25] Pioldi F, Rizzi E. Earthquake-induced structural response output-only identification by two different Operational Modal Analysis techniques. Earthq Eng Struct Dyn 2018;47:257–64. https://doi.org/10.1002/eqe.2947.
[26] Gersch W. On the achievable accuracy of structural system parameter estimates. J Sound Vib 1974;34:63–79. https://doi.org/10.1016/S0022-460X(74)80355-X.
[27] Gersch W, Nielsen NN, Akaike H. Maximum likelihood estimation of structural parameters from random vibration data. J Sound Vib 1973;31:295–308. https://doi.org/10.1016/S0022-460X(73)80274-3.
[28] Pintelon R, Guillaume P, Schoukens J. Uncertainty calculation in (operational) modal analysis. Mech Syst Signal Process 2007;21:2359–73. https://doi.org/10.1016/j.ymssp.2006.11.007.
[29] Au S. Uncertainty law in ambient modal identification — Part I: theory. Mech Syst Signal Process 2014;48:15–33. https://doi.org/10.1016/j.ymssp.2013.07.016.
[30] Hernandez E, Polanco N. A lower bound for the variance of frequency and damping ratio identified from noisy vibration measurements. Struct Control Heal Monit 2016;23:5–19. https://doi.org/10.1002/stc.1757.
[31] Hart G, Vasudevan R. Earthquake design of buildings: damping. J Struct Div 1975;101:11–30.
[32] Reinoso E, Miranda E. Estimation of floor acceleration demands in high-rise buildings during earthquakes. Struct Des Tall Spec Build 2005;14:107–30. https://doi.org/10.1002/tal.272.
[33] Caughey TK, O'Kelly MEJ. Classical normal modes in damped linear dynamic systems. J Appl Mech 1960;27:269–71. https://doi.org/10.1115/1.3643949.
[34] USGS, CGS, ANSS. Center for engineering strong motion data, < http://strongmotioncenter.org > , last accessed on 2015-08-01 2015. < http://strongmotioncenter.org > (accessed August 1, 2015).
[35] Stagner JR, Hart G. Damping estimation and digital filtering applied to structural motion studies. Report No. UCLA-ENG-7181. Los Angeles: University of California; 1971.
[36] Jeary AP. Damping in tall buildings - A mechanism and a predictor. Earthq Eng Struct Dyn 1986;14:733–50. https://doi.org/10.1002/eqe.4290140505.
[37] Shinozuka M, Ghanem R. Structural-system identification. II: experimental verification. J Eng Mech 1995;121:265–73.
[38] Miranda E, Taghavi S. Approximate floor acceleration demands in multistory buildings. I: formulation. J Struct Eng 2005;131:203–11.
[39] Chopra AK. Dynamics of structures: theory and applications to earthquake engineering. 4th ed. Upper Saddle River, NJ: Pearson Education, Inc.; 2012.
[40] Ljung L. System identification: theory for the user. Saddle River, NJ: Prentice-Hall; 1999.

Attachment B:

Generalized Random Decrement Method for Analysis of Vibration Data

P. D. Spanos
Ryon Chair in Engineering
Fellow ASME

B. A. Zeldin
Research Associate.

Department of Mechanical Engineering,
MS 321,
George R. Brown School of Engineering,
Rice University
Houston, TX 77251

The Random Decrement method used in system identification for analysis of random vibration data is considered from a rigorous mathematical perspective. It is shown that the Random Decrement signature deviates from the system free vibration curve of an associated linear system, unless the corresponding input excitation is white. The error induced by approximating the system excitation by a white noise process is examined. Further, a generalized Random Decrement signature is introduced; it is used to estimate efficiently the auto-correlation function of an ergodic Gaussian random process. Several examples are discussed to elucidate the theoretical developments.

1 Introduction

The Random Decrement method has been developed in industrial applications for estimating, from pertinent vibration records, the free vibration curves of randomly excited linear systems. A broad class of system identification techniques is based on this information. This method was introduced, on a rather heuristic basis, by Cole (1971, 1973) who sought a system signature which is not influenced by the parameters of the random excitation. Specifically, given a record of an ergodic stationary time series $x(t)$ which is related to the forced random vibration of a linear system, the determination of the free vibration curve of the system is pursued by selecting a reference level X_0 and recording the times at which the record crosses this level in both directions. Then, an ensemble of records is produced by cutting-off the segments of the record up to the crossing time, and re-initializing the time axis; the Random Decrement signature D_{X_0} is obtained by averaging this ensemble of generated records. The obtained "free vibration curve" can, then, be used to identify the parameters of the associated linear system (Cole, 1973; Ibrahim 1977, 1984; Jeary, 1986; Tamura et al., 1995; Marukawa, 1996; Kareem and Gurley, 1996). Several similar procedures for estimating approximately the system free vibration curves have been proposed under the generic name of the Random Decrement method.

Vandiver et al. (1982) presented an elementary mathematical justification for the application of the Random Decrement method for analyzing ergodic time series. The Random Decrement signature D_{X_0} was formally defined as

$$D_{X_0}(t_1, t_2) = E[x(t_2)|x(t_1) = X_0], \tag{1}$$

where $E[|]$ denotes the conditional expectation operator. For a Gaussian process $x(t)$ Eq. (1) yields

$$D_{X_0}(\tau) = X_0 R_x(\tau)/R_x(0), \tag{2}$$

where $R_x(\tau)$ is the auto-correlation function of the signal $x(t)$. Also, Vandiver et al. (1982) pointed out the obvious weaknesses of the arguments of references (Cole 1971, 1973; Ibrahim 1977) and showed by using Eqs. (1) and (2) that the Random Decrement signature D_{X_0} is proportional to the signal auto-correlation function $R_x(\tau)$ rather than to the system free vibration curve. However, Vandiver et al. (1982) associated, erroneously, the ensemble averaging concept used by Caughey and Stumpf (1961) for determining the nonstationary random response of linear systems with the time-averaging of ergodic processes in the Random Decrement method and questioned the validity of some of the results presented in Caughey and Stumpf (1961). Note that, nevertheless, the misconceived use of the Random Decrement signature as the system free vibration curve has continued in engineering applications (Ibrahim, 1984; Yang et al., 1985; Jeary 1986; Bedewi and Yang, 1987; Tamura, 1996).

This paper aims to clarify some theoretical and computational issues regarding the Random Decrement method. An approach is introduced to show that the Random Decrement signature can not be equal to the system free vibration curve if the random excitation is not white. Indeed, every response signature associated with a linear system is influenced by the parameters of the input excitation. Further, the error induced by the commonly used assumption that the excitation is white is analyzed, and the convergence of the Random Decrement signature to the system free vibration curve as the excitation tends to a white noise process is studied. Finally, a new Random Decrement signature is proposed for estimating the auto-correlation function of an ergodic process. Several examples are considered to elucidate the theoretical developments.

2 Random Decrement Signature and System Free Vibration

In conjunction with the preceding comments and to reflect on the point that the Random Decrement signature is influenced by the parameters of the colored excitation, two single-input-single-output linear systems with transfer functions $H_1(\omega)$ and $H_2(\omega)$ are considered. If these systems are excited by stationary random processes with spectral density functions

$$S_{u_1}(\omega) = |H_2(\omega)|^2, \tag{3}$$

and

$$S_{u_2}(\omega) = |H_1(\omega)|^2, \tag{4}$$

respectively, white noise input with unit spectral density can be assumed for the augmented systems shown in Fig. 1(*a*) and Fig. 1(*b*), respectively. Note that in this case the responses $x_1(t)$ and $x_2(t)$ of the combined systems are stochastically equivalent and have identical second order characteristics. Therefore, any response signature, in particular the Random Decrement signature, cannot distinguish the system parameters

Contributed by the Technical Committee on Vibration and Sound for publication in the JOURNAL OF VIBRATION AND ACOUSTICS. Manuscript received Aug. 1996. Associate Technical Editor: R. Ibrahim.

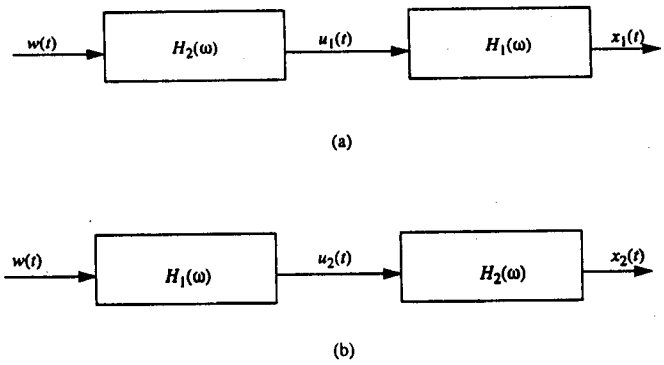

Fig. 1 Combined linear systems

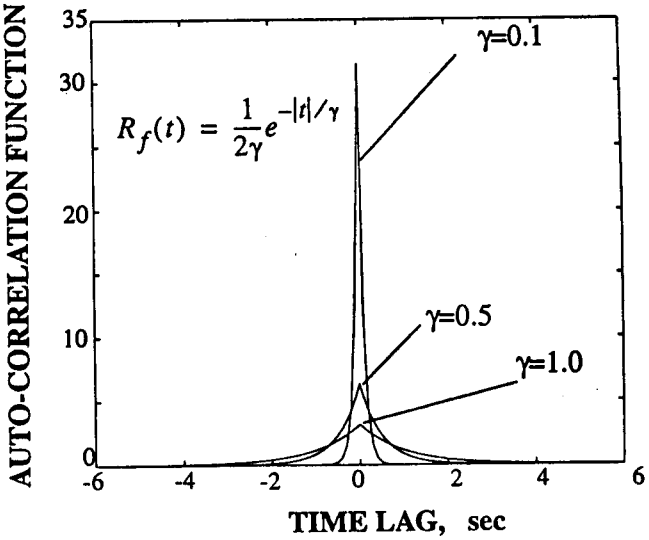

Fig. 2 Auto-correlation function versus time lag; various values of γ

from the excitation parameters using the response record alone. This conclusion is consistent with Eq. (2) for the Gaussian case, since in this case the Random Decrement signature is proportional to the auto-correlation function which represents a combination of the system and excitation parameters.

Often, processes used in engineering practice have spectra which are "broad" compared to the system transfer function. In this case assuming that the system excitation is a white noise process is a good approximation; this observation, perhaps, explains the moderate success of the Random Decrement method in certain applications. In this sense, if the system excitation is colored and the Random Decrement signature is assumed to represent the system free vibration curve, the error induced by this simplification must be properly evaluated. A rigorous treatment of a white noise process as a generalized stochastic process is given by Gel'fand and Vilenkin (1964) by extending the theory of generalized functions to the random case. In this paper, however, the simplified concept of a broad-sense white noise process (Wong, 1971) is used in conjunction with a second order analysis of the Random Decrement method. Specifically, the discrepancy between the process $f(t)$ and a wide-sense white noise process $w(t)$ of power λ^2 is represented by the norm

$$\|f(t) - w(t)\|_\alpha^2 = 2\pi \int_{-\infty}^{\infty} (1 + \omega^2)^{-\alpha} |\lambda^2 - S_f(\omega)|^2 d\omega, \quad (5)$$

where, since $S_f(\omega) \to 0$ as $\omega \to \infty$, the parameter α must be strictly larger than 0.5 for the integral in Eq. (5) to be well defined. Further, one can prove the following property regarding the convergence of the Random Decrement signature to the free vibration curve.

Property. Let $x_f(t)$ and $x_w(t)$ be the stationary responses of a linear system with the transfer function $H(\omega)$ to colored random excitation $f(t)$ and to white noise $w(t)$, respectively. If $H(\omega)$ is such that

$$[\max_\omega (1 + \omega^2)^\alpha |H(\omega)|^4]^{1/2} = C_1 < \infty, \quad (6)$$

or

$$\left(\frac{1}{2\pi} \int_{-\infty}^{\infty} (1 + \omega^2)^\alpha |H(\omega)|^4 d\omega\right)^{1/2} = C_2 < \infty, \quad (7)$$

for some $\alpha > 0.5$, then

$$\left(\int_{-\infty}^{\infty} (R_{x_f}(t) - R_{x_w}(t))^2 dt\right)^{1/2} \le C_1 \|f(t) - w(t)\|_\alpha, \quad (8)$$

or

$$\max_t |R_{x_f}(t) - R_{x_w}(t)| \le C_2 \|f(t) - w(t)\|_\alpha, \quad (9)$$

respectively.

A proof of this property is given in Appendix A. Thus, under merely weak conditions the auto-correlation function of the response of a linear system driven by an arbitrary stationary excitation tends absolutely and in the mean square sense to the auto-correlation function of the white noise response of the same system. Correspondingly, the deviation of the Random Decrement signature from the system free vibration curve becomes negligible; the rate of this convergence depends on the convergence of the colored excitation to a white noise process. Note that linear systems with proper rational transfer functions satisfy the conditions of Eqs. (6) and (7). Equations (8) and (9) provide useful explicit bounds on the expected error of the white noise approximation. To illustrate the above property consider the following example.

Example 1. Assume that the input excitation $f(t)$ has auto-correlation function and associated spectral density function

$$R_f(t) = \frac{\pi}{\gamma} \exp\left(-\frac{|t|}{\gamma}\right) \quad (10)$$

and

$$S_f(\omega) = \frac{1}{\omega^2\gamma^2 + 1}, \quad -\infty < \omega < \infty, \quad (11)$$

respectively. The auto-correlation function of Eq. (10) and the spectral density function of Eq. (11) are plotted for several values of γ in Fig. 2 and Fig. 3, respectively. Clearly, the process $f(t)$ becomes white noise, with $\lambda^2 = 1$, as $\gamma \to 0$. Indeed,

$$\begin{aligned}
&\|f(t) - w(t)\|_\alpha^2 \\
&= 2\pi \int_{-\infty}^{\infty} \frac{1}{(1 + \omega^2)^\alpha} |S_f(\omega) - 1|^2 d\omega \\
&= 2\pi \int_{-\infty}^{\infty} \frac{\omega^4\gamma^4}{(1 + \omega^2)^\alpha(\omega^2\gamma^2 + 1)^2} d\omega \\
&= 4\pi\left(\int_0^1 + \int_1^{1/\alpha} + \int_{1/\alpha}^{\infty}\right) \\
&\le 4\pi\left(\gamma^4 \int_0^1 \omega^4 d\omega + \gamma^4 \int_1^{1/\gamma} \omega^{4-2\alpha} d\omega\right)
\end{aligned}$$

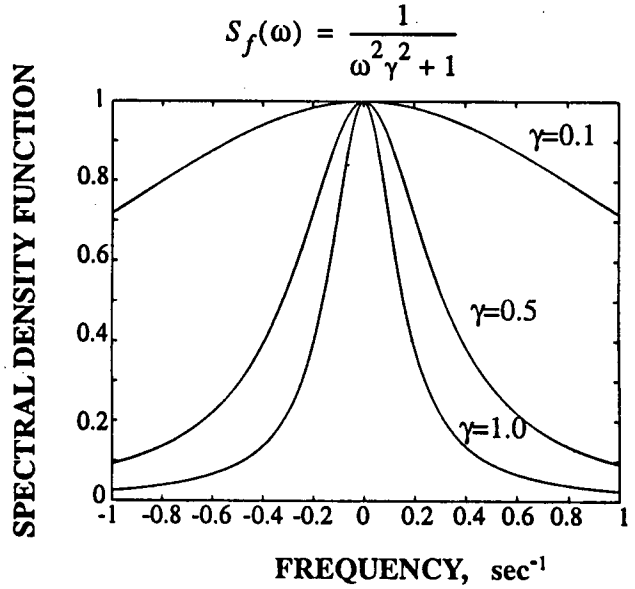

Fig. 3 Spectral density functions versus frequency; various functions of γ

$$+ \int_{1/\gamma}^{\infty} \frac{1}{(1+\omega^2)^{\alpha}}\, d\omega \Bigg)$$

$$= \begin{cases} C\gamma^4 + C\gamma^{2\alpha-1}, & 2\alpha \neq 5 \\ C\gamma^4 + C\gamma^{2\alpha-1}|\ln\gamma| + C\gamma^{2\alpha-1}, & 2\alpha = 5 \end{cases} \quad \alpha > 0.5. \tag{12}$$

Equation (12) demonstrates that the rate of convergence of the excitation towards white noise depends on the norm with respect to which this convergence is measured; this convergence is faster for larger values of α.

Next, consider the response of a subcritically damped single-degree-of-freedom oscillator to $f(t)$; the equation of motion is

$$x''(t) + 2\xi\omega_0 x'(t) + \omega_0^2 x(t) = f(t). \tag{13}$$

The transfer function of this linear system and the auto-correlation function of its response to white noise with unit two-sided spectral density are

$$H(\omega) = \frac{1}{\omega_0^2 - \omega^2 + 2i\xi\omega_0\omega}, \tag{14}$$

and

$$R_{x_w}(\tau) = R_{x_w}(0)e^{-\xi\omega_0|\tau|}\left(\cos\omega_d|\tau| + \frac{\xi\omega_0}{\omega_d}\sin\omega_d|\tau|\right), \tag{15}$$

where $\omega_d = \omega_0\sqrt{1-\xi^2}$ and $R_{x_w}(0) = \pi/2\xi\omega_0^3$. If the input excitation is not white but rather has the second moment properties given by Eqs. (10) and (11), the auto-correlation function of the system response is

$$R_{x_f}(\tau) = R_{x_w}(0)\left\{e^{-\xi\omega_0|\tau|}\left(c_1(\gamma)\cos\omega_d|\tau| + c_2(\gamma)\frac{\xi\omega_0}{\omega_d}\sin\omega_d|\tau|\right) + 2\gamma^3\xi\omega_0^3 c_3(\gamma)e^{-|\tau|/\gamma}\right\} \tag{16}$$

where

$$c_1(\gamma) = (1 + \gamma^2\omega_0^2(1 - 4\xi^2))/d(\gamma), \tag{17}$$

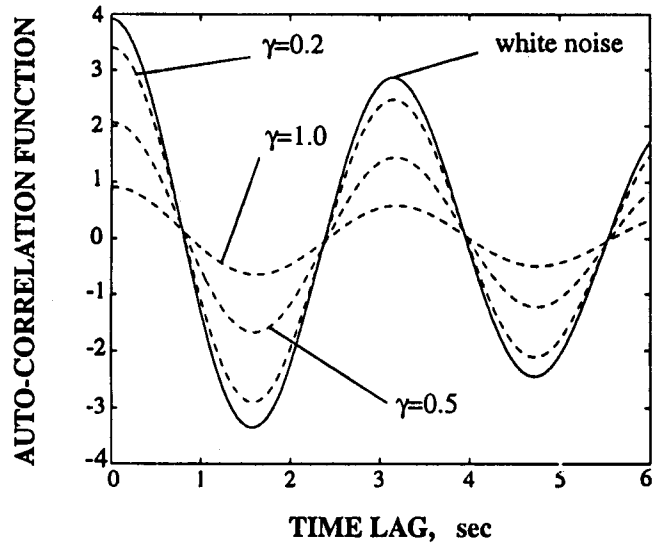

Fig. 4 Auto-correlation function of the system versus time; various values of γ

$$c_2(\gamma) = (1 + \gamma^2\omega_0^2(3 - 4\xi^2))/d(\gamma), \tag{18}$$

and

$$c_3(\gamma) = 1/d(\gamma) \tag{19}$$

with

$$d(\gamma) = (1 + \gamma^2\omega_0^2(1 - 4\xi^2))^2 + 4\gamma^4\omega_0^4\xi^2(1 - \xi^2). \tag{20}$$

Equations (17)–(19) show that c_1, c_2, and c_3 tend to 1 as $\gamma \to 0$. Then, $R_{x_f}(t)$ converges to $R_{x_w}(t)$ consistently with the preceding property. Figure 4 shows the function $R_{x_f}(\tau)$ for several values of γ, and for ω_0, ξ equal to 2 and 0.05, respectively. The rate of the convergence of $R_{x_f}(t)$ to $R_{x_w}(t)$ is shown in Fig. 5 where the maximum difference between these two auto-correlation functions is plotted versus $1/\gamma$. In this regard, it is pointed out that for the transfer function given by Eq. (14) one can select the value of α up to 3.5 according to the condition

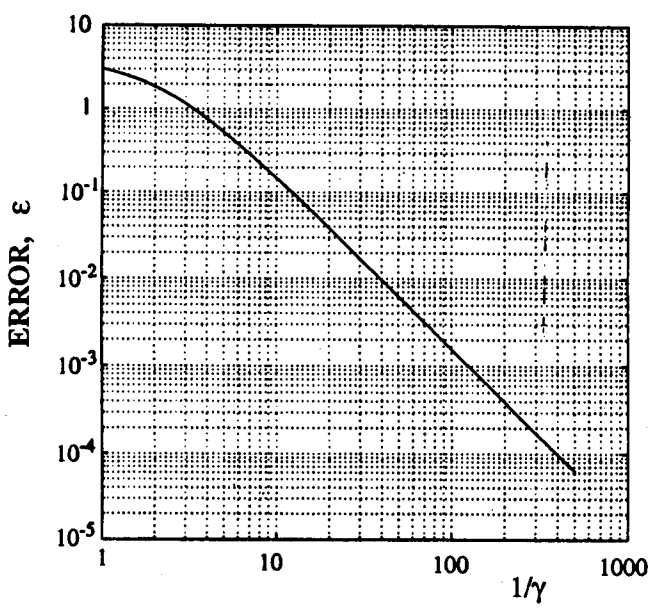

Fig. 5 Absolute error of the approximation of the auto-correlation function versus $1/\gamma$; $\epsilon = \max_t |R_{x_f}(t) - R_{x_w}(t)|$

of Eq. (7). Then, Eq. (12) yields that the absolute error tends to zero with the rate γ^2; this is clearly shown in Fig. 5.

3 A New Random Decrement Procedure: An Efficient Estimate of the Auto-Correlation Function

3.1 Theoretical Developments. Vandiver et al. (1982) showed that the numerical algorithm of reference (Cole, 1973) yields the auto-correlation function for an ergodic Gaussian process $x(t)$. Next, the numerical efficiency of estimating the auto-correlation function by using the Random decrement method is considered. Let the symbol $x_i = x(i\Delta t)$ denote the value of the process $x(t)$ at the time moment $i\Delta t$, where Δt is the sampling time. Correspondingly, $R(k) = E[x_i x_{i+k}]$ denotes the value of the auto-correlation function at the time lag $k\Delta t$. Then, the numerical algorithm of reference (Cole, 1973) can be expressed as

$$\overline{D_{X_0}}(k) = \frac{1}{M}\sum_{i=1}^{N} \eta_{X_0}(x_i)x_{i+k} \tag{21}$$

where the bar indicates the estimated value rather than exact, N is the number of the sampled points in the record of $x(t)$, and

$$\eta_{X_0}(x) = \begin{cases} 1, & x \in \left[X_0 - \dfrac{\Delta x}{2}, X_0 + \dfrac{\Delta x}{2}\right] \\ 0, & \text{otherwise} \end{cases}. \tag{22}$$

Further, Δx denotes the size of the interval around the selected reference level X_0, and M is the number of points that belong to the interval $[X_0 - (\Delta x/2), X_0 + (\Delta x/2)]$. If the length Δx is sufficiently small and N is large one can set

$$\frac{M}{N} \approx p_x(X_0)\Delta x. \tag{23}$$

Thus, the Random Decrement signature of Eq. (21) is approximately equal to

$$D_{X_0}(k) = \frac{1}{p_x(X_0)\Delta x} E[x_i \eta_{X_0}(x_{i-k})]. \tag{24}$$

In the limit, as Δx tends to zero, Eq. (24) becomes

$$D_{X_0}(k) = \frac{1}{p_x(X_0)} E[x_i \delta(x_{i-k} - X_0)], \tag{25}$$

where $\delta(x)$ is the Dirac delta-function. It can be readily shown that the mathematical definitions of the Random Decrement signature given by Eqs. (1) and (25) coincide. Indeed,

$$\begin{aligned} &\frac{1}{p_x(X_0)} E[x_1 \delta(x_2 - X_0)] \\ &= \frac{1}{p_x(X_0)} \iint x_1 \delta(x_2 - X_0) p_{x_1,x_2}(x_1, x_2) dx_1 dx_2 \\ &= \int x_1 \frac{p_{x_1,x_2}(x_1, X_0)}{p_{x_2}(X_0)} dx_1 = \int x_1 p_{x_1|x_2}(x_1 | x_2 = X_0)\, dx_1 \\ &= E[x_1 | x_2 = X_0]. \end{aligned} \tag{26}$$

However, the definition given by Eq. (25) is amenable to a generalization.

The Random Decrement method based on Eq. (21) is a computationally expedient procedure, since it requires to perform only M summations for every time lag k. However, it "wastes" a significant part of the response record since only very few points fall in the interval $[X_0 - (\Delta x/2), X_0 + (\Delta x/2)]$. Thus, the Random Decrement signature of Eq. (21) cannot be used when the response record is short. To remedy this problem the definition of Eq. (25) can be generalized by substituting the function sgn (x) in place of the Dirac delta-function, where

$$\text{sgn}\,(x) = \begin{cases} 1, & x > 0 \\ 0, & x = 0 \\ -1, & x < 0 \end{cases} \tag{27}$$

is the sign function. This leads to the estimate

$$\bar{D}(i) = \frac{1}{N}\sum_{k=0}^{N-1} \text{sgn}\,(x_k)x_{k+i}, \tag{28}$$

which utilizes the entire length of the record. Also, this new estimate still requires to perform only summations similar to the original Random Decrement method. In this regard, it is pointed out that Eq. (28) can be seen as the average, over all possible reference levels, of an ensemble of Random Decrement signatures of Eq. (21). Interestingly, Eq. (28) was originally introduced in electrical engineering literature (Hertz, 1982) from a pure signal processing perspective.

For ergodic Gaussian process, the generalized Random Decrement signature of Eq. (28) is a random variable. The quality of the Random Decrement estimation can be assessed by evaluating the mean and the variance of this random variable. In this regard its mean value can be readily found as

$$\begin{aligned} E[\bar{D}(i)] &= \frac{1}{N}\sum_{k=0}^{N-1} E[x(k+i)\,\text{sign}\,(x(k))] \\ &= E[x(i)\,\text{sgn}\,(x(0))]. \end{aligned} \tag{29}$$

In the Gaussian case the mathematical expectation operator in the right-hand side of Eq. (29) can be simplified by using the formula

$$E[xg(y)] = E[xy]E\left[\frac{d}{dy} g(y)\right], \tag{30}$$

where x and y are jointly Gaussian and $g(x)$ is an arbitrary function; see Roberts and Spanos (1990). Substituting Eq. (27) into Eq. (30) yields

$$\begin{aligned} E[\bar{D}(i)] &= E[x(k+i)x(k)]E\left[\frac{d}{dx}\,\text{sign}\,(x(k))\right] \\ &= C\sigma^2\rho(i), \end{aligned} \tag{31}$$

where σ^2 and $\rho(i)$ denote the variance and the auto-correlation function, normalized to one for zero time lag, of the process $x(t)$, respectively, and

$$C = E\left[\frac{d}{dx}\,\text{sign}\,(x(k))\right] = 2E[\delta(x(k))] = \sqrt{\frac{2}{\pi}}\frac{1}{\sigma}. \tag{32}$$

Thus, the generalized Random Decrement signature is an unbiased estimate of the shape of the auto-correlation function. Then, upon evaluating the Random Decrement signature by using Eq. (28), the auto-correlation function can be estimated by the equation

$$\overline{R_D}(k) = \frac{\pi}{2}\bar{D}(0)\bar{D}(k). \tag{33}$$

Further, the variance of the generalized Random Decrement estimate can be determined after some rather tedious mathematical calculations summarized in Appendix B. Specifically,

$$\begin{aligned} &\text{Var}\,(\bar{D}(i)) \\ &= E[\bar{D}^2(i)] - E[\bar{D}(i)]^2 \\ &= \frac{\sigma^2}{N}\left(1 - \frac{2}{\pi}\rho(i)^2\right) + \frac{4\sigma^2}{\pi N}\sum_{k=1}^{N-1}\left(1 - \frac{k}{N}\right)\rho_D(k, i), \end{aligned} \tag{34}$$

where

$$\rho_D(k, i) = \rho(k) \operatorname{asin}(\rho(k)) + \frac{\rho(i)^2 + \rho(k+i)\rho(k-i) - (\rho(k+i) + \rho(k-i))\rho(k)\rho(i)}{\sqrt{1-\rho(k)^2}} - \rho(i)^2. \quad (35)$$

It is even more cumbersome to evaluate the variance of the estimate of Eq. (33). In this regard one can argue that by virtue of the Central Limit Theorem, the generalized Random Decrement signature $\bar{D}(k)$ of Eq. (28) tends to exhibit Gaussian properties (Ditlevsen et al., 1996; Mohr and Ditlevsen, 1996). Then, with probability 95.5 percent for the estimate of Eq. (28) it can be argued that

$$\bar{D}(i) \in [D(i) - 2\sqrt{\operatorname{Var}(D(i))}, \; D(i) + 2\sqrt{\operatorname{Var}(D(i))}]. \quad (36)$$

Similarly, with probability 95.5 percent for the estimate of Eq. (33) it can be argued that

$$\overline{R_D}(i) \in [R(i) - 2\nu_D(i), R(i) + 2\nu_D(i)], \quad (37)$$

where

$$\nu_D(i) = \sqrt{\frac{\pi}{2}}\left(\sigma|\rho(i)|\sqrt{\operatorname{var}(\hat{D}(0))} + \sigma\sqrt{\operatorname{var}(\hat{D}(i))}\right). \quad (38)$$

Therefore, the variance of the estimate $\overline{R_D}(k)$ can be approximated by the equation

$$\operatorname{Var}(\overline{R_D}(i)) \approx \nu_D(i)^2 \quad (39)$$

3.2 Computational Efficiency. Next, the usefulness of the generalized Random Decrement signature can be assessed by comparing it with the standard estimate of the auto-correlation function which is commonly used in engineering applications. Specifically, consider the expression

$$\overline{R_2}(i) = \frac{1}{N}\sum_{k=0}^{N-1} x(k+i)x(k), \quad i = 0, 1, \ldots M-1. \quad (40)$$

Comparing Eqs. (28) and (40) it is seen that Eq. (40) requires twice, roughly, as many computations (N multiplications and $N-1$ additions) as the generalized Random Decrement signature does. The variance of the estimate of Eq. (40) can be readily determined in the Gaussian case. Specifically,

$$\operatorname{Var}(\hat{R}_2(i)) = \frac{\sigma^4}{N}(1 + \rho^2(i)) + \frac{2\sigma^4}{N}\sum_{k=1}^{N-1}\left(1 - \frac{k}{N}\right)\rho_2(k, i), \quad (41)$$

where

$$\rho_2(k, i) = \rho(k)^2 + \rho(k+i)\rho(k-i). \quad (42)$$

Evidently, the variance of the estimates of the auto-correlation function given by Eq. (39) or Eq. (41) is approximately proportional to $1/N$. Further, the number of computations (flops) required by Eqs. (33) and (40) is also proportional to N. Then, the parameter κ defined by the equation

$$\kappa = \operatorname{Var}(\bar{R}) \cdot \#\text{flops} \quad (43)$$

is approximately equal to a constant and can be used to determine the number of required computations for ensuring a specified error bound. In the following examples the variances of the estimates of the auto-correlation function of Eqs. (33) and (40) are evaluated numerically and the corresponding values of the parameter κ are found.

Example 2. Consider the Gaussian white noise signal. That is, the sequence of zero mean, Gaussian, and uncorrelated random variables. Then,

$$\rho(i) = \delta_{0,i}, \quad (44)$$

where $\delta_{i,j}$ is the Kronecker delta. Utilizing Eqs. (34), (35), (38), (39), (41), (42), and (44), the variance of the corresponding estimates is found equal to

$$\operatorname{Var}(\overline{R_D}(0)) \approx 4\left(\frac{\pi}{2} - 1\right)\frac{\sigma^4}{N} = \frac{2.2832}{N}\sigma^2 > \frac{2\sigma^2}{N} = \operatorname{Var}(\overline{R_2}(0)). \quad (45)$$

Thus, the standard estimate of Eq. (40) is more accurate for this problem. This result should be expected since the estimate (40) is an "efficient estimate" (Cramer, 1946) in this case. That is, it attains the lowest Cramer-Rao bound and has the smallest variance among all possible unbiased estimates (Cramer, 1946). On the other hand, the estimate of Eq. (33) requires to perform only N numerical operations, $N-1$ additions and 1 multiplication, whereas the estimate of Eq. (40) requires $2N-1$ numerical operation. The parameter κ, Eq. (43), is equal to 2.28 for the Random Decrement based estimation, and is equal to 4 for the standard estimation procedure of Eq. (40). That is, the requisite calculations can be performed approximately 40 percent faster by using the generalized Random Decrement signature.

Example 3. Consider a stationary process with the auto-correlation function

$$R(t) = \sigma^2 e^{-\xi\omega_0|\tau|}\left(\cos\omega_d|\tau| + \frac{\xi\omega_0}{\omega_d}\sin\omega_d|\tau|\right), \quad (46)$$

This auto-correlation function corresponds to the white noise response of a simple oscillator governed by Eq. (13). The values of σ, ω_0, ξ, Δt and N are taken equal to 1, 2, 0.05, 0.05 and 5000, respectively. The variance of the estimates of Eqs. (33) and (40) are shown in Fig. 6. Similarly to the previous example, the direct estimate of the auto-correlation function of equation (40) provides a slightly smaller variance of estimation. However, Fig. 7 shows the ratio κ_D/κ_2 for these two estimates versus the time lag i. It appears that the estimate of the auto-correlation function which is based on the generalized Random Decrement signature is, on average, 40 percent more expeditious computationally.

4 Conclusions

The developed analytical results elucidate the approximations involved in using the Random Decrement signature for system identification purposes while treating the system excitation as a white noise process. Further, the erroneous interpretation of the results of Caughey and Stumpf (1961) invoked by Vandiver et al. (1982) for understanding the features of the Random Decrement signature is rectified. Also, the introduction of the generalized Random Decrement signature as an average of the

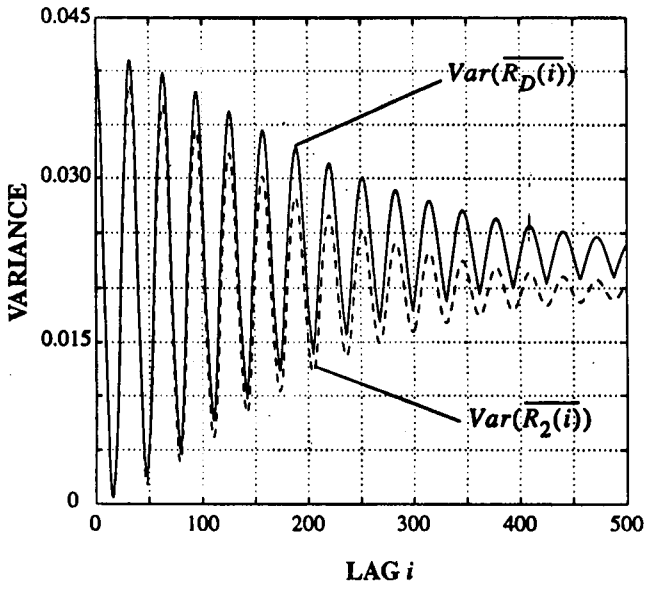

Fig. 6 Variance of the estimate of the auto-correlation function; Eqs. (39) and (41)

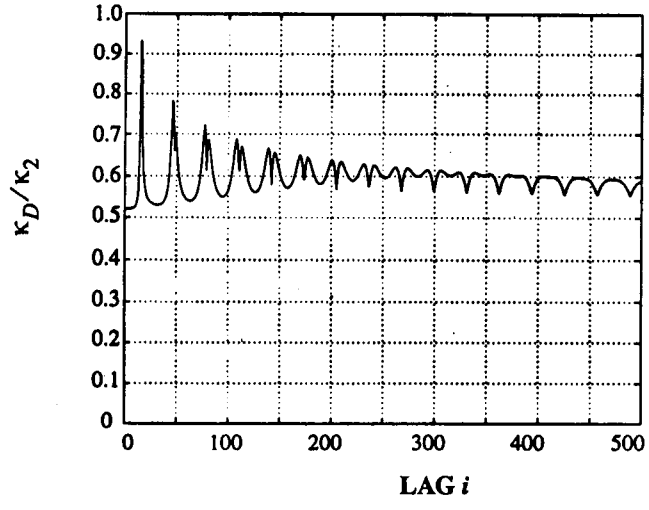

Fig. 7 The ratio of the variances multiplied by the required numerical operations of the estimates of the auto-correlation function of Eqs. (33) and (40)

traditional Random Decrement signatures, over the possible thresholds, yields an expeditious estimate of the auto-correlation function which coincides with the definition independently proposed in electrical engineering from a pure signal processing perspective. Finally, the expression derived for the variance of this estimate merits attention.

Acknowledgment

The financial support of this work by the grant DE-FG03-95ER14500 from the Department of Energy is gratefully acknowledges.

References

1 Bedewi, N. E., and Yang, J. C. S., 1987, "System Identification Technique Based on the Random Decrement Signatures, Part I: Theory and Simulation," *NASA Conference Publication 58th Shock and Vibration Symposium*, Huntsville, AL, Vol 1, pp. 277–273.

2 Caughey, T. K., and Stumpf, H. J., 1961, "Transient Response of a Dynamic System Under Random Excitation," ASME *Journal of Applied Mechanics*, Vol. 28, No. 4, pp. 563–566.

3 Cole, H. A., 1971, "Failure Detection of a Space Shuttle Wing Flutter Model by Random Decrement," *NASA Report* TM X-62041.

4 Cole, H. A., 1973, "On-Line Failure Detection and Damping Measurement of Aerospace Structures by Random Decrement Signatures," *NASA Report* CR-2205.

5 Cramer, H., 1946, *Mathematical Methods of Statistics*, Princeton University Press, Princeton, New Jersey.

6 Ditlevsen, O., Mohr, G., and Hoffmeyer, P., (1996). "Integration of Non-Gaussian Fields," *Probabilistic Engineering Mechanics*, Vol. 11, No. 1, pp. 15–23.

7 Gel'fand, I. M., and Vilenkin, N. Y., 1964, *Generalized Functions* (Volume 4), Academic Press, New York.

8 Gradshtein, I. S., and Ryzhik, I. M., 1994, *Tables of Integrals, Series, and Products*, Academic Press, New York.

9 Hertz, D., 1982, "A Fast Digital Method of Estimating the Autocorrelation of A Gaussian Stationary Process," *IEEE Transactions on Acoustics, Speech and Signal Processing*, ASSP-Vol. 30, No. 2, pp. 329.

10 Ibrahim, S. R., 1977, "Random Decrement Technique for Modal Identification of Structures," *Journal of Spacecraft*, No. 14, Vol. 11, pp. 696–700.

11 Ibrahim, S. R., 1984, "Incipient Failure Detection from Random Decrement Time Functions," *Random Vibration*, T. C. Huang and P. D. Spanos, eds., AMD-65, 69–81.

12 Jeary, A. P., 1986, "Damping in Tall Buildings—A Mechanism and A Predictor," *Earthquake Engineering and Structural Dynamics*, Vol. 14, pp. 733–750.

13 Kareem, A., and Gurley, K., 1996, "Damping in Structures: Its Evaluation and Treatment of Uncertainty," *Journal of Wind Engineering and Industrial Aerodynamics*, Vol. 59, pp. 131–157.

14 Lin, Y. K., 1976, *Probabilistic Theory of Structural Dynamics*, Robert E Krieger Publishing Company, Huntington, New York.

15 Marukawa, H., Kato, N., Fujii, K., and Tamura, Y., 1996, "Experimental Evaluation of Aerodynamic Damping of Tall Building," *Journal of Wind Engineering and Industrial Aerodynamics*, Vol. 59, pp. 177–190.

16 Mohr, G., and Ditlevsen, O., 1996, "Partial Summations of Stationary Sequences of Non-Gaussian Random Variables," *Probabilistic Engineering Mechanics*, Vol. 11, No. 1, pp. 25–30.

17 Roberts, J. B., and Spanos, P. D., 1990, *Random Vibration and Statistical Linearization*, John Wiley and Sons, Inc., New York.

18 Tamura, Y., Fujii, K., Ohtsuki, T., Wakahara, T., and Kohsaka, R., 1995, "Effectiveness of Tuned Liquid Dampers under Wind Excitation," *Engineering Structures*, Vol. 17, No. 9, pp. 609–621.

19 Vandiver, J. K., Dunwoody, A. B., Campbell, R. B., and Cook, M. F., 1982, "A Mathematical Basis for the Random Decrement Vibration Signature Analysis Technique," ASME *Journal of Mechanical Design*, Vol. 104, No. 4, pp. 307–313.

20 Wong, E., 1971, *Stochastic Processes in Information and Dynamic Systems*, McGraw-Hill, New York.

21 Yang, J. C. S., Marks, C. H., Jiang, J., Chen, D., Elahi, A., and Tsai, W.-H., 1985, "Determination of Fluid Damping Using Random Excitation," *Journal of Energy Resources Technology*, Vol. 107, pp. 220–225.

APPENDIX A

This appendix presents the proof of the property involved in Section 2. In this regard, it is noted that the stationary responses $x_f(t)$ and $x_w(t)$ of a linear system with the transfer function $H(\omega)$ to the colored random excitation $f(t)$ and to the white noise $w(t)$ of power λ^2 have the spectral density functions

$$S_{x_f}(\omega) = |H(\omega)|^2 S_f(\omega), \tag{A.1}$$

and

$$S_{x_w}(\omega) = |H(\omega)|^2 \lambda^2, \tag{A.2}$$

respectively. Note that due to the Parseval identity for the Fourier transform couple $R(t)$ and $S(\omega)$ one can write

$$\int_{-\infty}^{\infty} |R(t)|^2 dt = 2\pi \int_{-\infty}^{\infty} |S(\omega)|^2 d\omega \tag{A.3}$$

Then, the mean square discrepancy between the auto-correlation functions $R_{x_f}(t)$ and $R_{x_w}(t)$ can be found as

$$\int_{-\infty}^{\infty} (R_{x_f}(t) - R_{x_w}(t))^2 dt$$

$$= 2\pi \int_{-\infty}^{\infty} |S_{x_f}(\omega) - S_{x_w}(\omega)|^2 d\omega$$

$$= 2\pi \int_{-\infty}^{\infty} |H(\omega)|^4 |S_f(\omega) - \lambda^2|^2 d\omega$$

$$\leq \max\{(1+\omega^2)^{\alpha}|H(\omega)|^4\} \times 2\pi \int_{-\infty}^{\infty} (1+\omega^2)^{-\alpha}|S_f(\omega)-\lambda^2|^2 d\omega$$

$$= \max\{(1+\omega^2)^{\alpha}|H(\omega)|^4\}\|f(t)-w(t)\|_{\alpha}^2, \quad \text{(A.4)}$$

If $H(\omega)$ is bounded and decays at infinity sufficiently fast so that

$$(\max\,(1+\omega^2)^{\alpha}|H(\omega)|^4)^{1/2} = C_1 < \infty \quad \text{(A.5)}$$

for some $\alpha > 0.5$, the upper bound of the mean square error is

$$\left(\int_{-\infty}^{\infty} (R_{x_f}(t) - R_{z_w}(t))^2 dt\right)^{1/2} \leq C_1\|f(t)-w(t)\|_{\alpha}. \quad \text{(A.6)}$$

The equality sign in Eq. (A.6) is attained for the random excitation $f(t)$ with the spectral density function

$$S_f(\omega) = \begin{cases} \lambda^2 + C, & |\omega \pm \omega_0| < \eta \\ \lambda^2, & \text{otherwise} \end{cases}, \quad \text{(A.7)}$$

in the extreme case when $\eta \to 0$. Here, ω_0 is the frequency at which the function $(1+\omega^2)^{\alpha}|H(\omega)|^4$ attains its maximum, C is an arbitrary constant, and η is a small parameter.

The absolute error between the two auto-correlation functions can be also readily found

$$\max|R_{x_f}(t) - R_{z_w}(t)| = \max\left|\int_{-\infty}^{\infty} (S_{x_f}(\omega) - S_{x_w}(\omega))e^{i\omega t} d\omega\right|$$

$$\leq \int_{-\infty}^{\infty} |H(\omega)|^2 |S_f(\omega)-\lambda^2|\, d\omega \times \left(\int_{-\infty}^{\infty} (1+\omega^2)^{\alpha}|H(\omega)|^4 d\omega\right)^{1/2} \times \left(\int_{-\infty}^{\infty} (1+\omega^2)^{-\alpha}|S_f(\omega)-\lambda^2|^2 d\omega\right)^{1/2}$$

$$= \left(\frac{1}{2\pi}\int_{-\infty}^{\infty} (1+\omega^2)^{\alpha}|H(\omega)|^4 d\omega\right)^{1/2} \|f(t)-w(t)\|_{\alpha}. \quad \text{(A.8)}$$

If $H(\omega)$ is such that

$$\left(\frac{1}{2\pi}\int_{-\infty}^{\infty} (1+\omega^2)^{\alpha}|H(\omega)|^4 d\omega\right)^{1/2} = C_2 < \infty \quad \text{(A.9)}$$

for some $\alpha > 0.5$, the absolute error satisfies the inequality

$$\max|R_{x_f}(t) - R_{z_w}(t)| \leq C_2\|f(t)-w(t)\|_{\alpha}. \quad \text{(A.10)}$$

Again the spectral density function $S_f(\omega)$ which provides the equality in Eq. (A.10) can be readily determined by the equation

$$S_f(\omega) = \lambda^2 + C(1+\omega^2)^{\alpha}|H(\omega)|^2, \quad \text{(A.11)}$$

where C is an arbitrary constant.

APPENDIX B

This mathematical appendix adresses the computation of the mathematical expectation of the product x_1x_2 sgn (x_3) sgn (x_4), where x_1, x_2, x_3, x_4 are zero mean Gaussian random variables with covariance matrix

$$r = \sigma^2 \begin{bmatrix} 1 & \rho_{12} & \rho_{13} & \rho_{14} \\ \rho_{12} & 1 & \rho_{23} & \rho_{24} \\ \rho_{13} & \rho_{23} & 1 & \rho_{34} \\ \rho_{14} & \rho_{24} & \rho_{34} & 1 \end{bmatrix}. \quad \text{(B.1)}$$

It has the appealing feature of taking advantages of the simplification induced by working with the characteristic function of the random vector $\underline{x} = (x_1, x_2, x_3, x_4)'$ (Lin 1976), where $(\,)'$ denotes vector transposition. Specifically, consider the equation

$$E[f(\underline{x})] = \int f(\underline{x})p(\underline{x})d\underline{x} = \frac{1}{(2\pi)^n}\int \hat{f}(\underline{\theta})\hat{p}(\underline{\theta})d\underline{\theta}, \quad \text{(B.2)}$$

where $p(\underline{x})$ and $p(\underline{\theta})$ are the probability distribution function and the characteristic function, respectively. The hat denotes the symbol of the Fourier transform. That is,

$$\hat{p}(\underline{\theta}) = \int_{-\infty}^{\infty} p(\underline{x})e^{-i\underline{\theta}'\underline{x}}\, d\underline{x}. \quad \text{(B.3)}$$

Further, note that

$$\hat{x} = 2\pi i\delta'(\theta), \quad \widehat{\text{sgn}(x)} = -2i\left(pv\,\frac{1}{\theta}\right),$$

$$\hat{p}(\underline{x}) = e^{-(1/2)\underline{\theta}'r\underline{\theta}}, \quad \text{(B.4)}$$

where $\delta'(\theta)$ denotes the derivative of the Dirac delta-function, and $pv\,(1/\theta)$ is the principal value functional of the argument. Then, the mathematical expectation of x_1x_2 sgn (x_3) sgn (x_4) can be expressed as

$$E[x_1x_2 \text{ sgn } (x_3) \text{ sgn } (x_4)] = \frac{1}{\pi^2} pv\int_{-\infty}^{\infty} pv\int_{-\infty}^{\infty} \frac{1}{\theta_3\theta_4}\frac{\partial^2}{\partial\theta_1\partial\theta_2} \times \exp\left(-\frac{1}{2}\underline{\theta}'r\underline{\theta}\right)\Big|_{\substack{\theta_1=0 \\ \theta_2=0}} d\theta_3 d\theta_4$$

$$= -\frac{\sigma^2\rho_{12}}{\pi^2} pv\int_{-\infty}^{\infty} pv\int_{-\infty}^{\infty} \frac{1}{\theta_3\theta_4} e^{-(\sigma^2/2)(\theta_3^2+\theta_3\theta_4\rho_{34}+\theta_4^2)} d\theta_3 d\theta_4 + \frac{\sigma^4\rho_{13}\rho_{23}}{\pi^2} pv\int_{-\infty}^{\infty}\int_{-\infty}^{\infty} \frac{\theta_3}{\theta_4} e^{-(\sigma^2/2)(\theta_3^2+\theta_3\theta_4\rho_{34}+\theta_4^2)} d\theta_3 d\theta_4 + \frac{\sigma^4\rho_{14}\rho_{24}}{\pi^2} pv\int_{-\infty}^{\infty}\int_{-\infty}^{\infty} \frac{\theta_4}{\theta_3} e^{-(\sigma^2/2)(\theta_3^2+\theta_3\theta_4\rho_{34}+\theta_4^2)} d\theta_3 d\theta_4 + \frac{\sigma^4(\rho_{13}\rho_{24}+\rho_{14}\rho_{23})}{\pi^2} \times \int_{-\infty}^{\infty}\int e^{-(\sigma^2/2)(\theta_3^2+\theta_3\theta_4\rho_{34}+\theta_4^2)} d\theta_3 d\theta_4. \quad \text{(B.5)}$$

The first integral in the right hand side of Eq. (B.5) can be evaluated by consulting the table of integrals (Gradshtein and Ryzhik, 1994) and using the following transformation

$$\left(-\frac{1}{\pi^2}\right) pv\int_{-\infty}^{\infty} pv\int_{-\infty}^{\infty} \frac{1}{\theta_1\theta_2} e^{-(\sigma^2/2)(\theta_1^2+\theta_1\theta_2\rho+\theta_2^2)} d\theta_1 d\theta_2$$

$$= \frac{1}{2\pi\sigma^2\sqrt{1-\rho^2}}\int_{-\infty}^{\infty}\int \text{sgn } (x_1) \text{ sgn } (x_2) \times \exp\left(-\frac{x_1^2 - 2x_1x_2\rho + x_2^2}{2\sigma^2(1-\rho^2)}\right) dx_1 dx_2$$

$$= \frac{1}{\sqrt{2\pi}\,\sigma}\int_{-\infty}^{\infty} \text{sgn } (x)\left(1 - 2\Phi\left(-\frac{x\rho}{\sigma\sqrt{1-\rho^2}}\right)\right)$$

$$\times \exp\left(-\frac{x^2}{2\sigma^2}\right)dx = \frac{4}{\sqrt{2\pi}}\int_0^\infty \Phi\left(\frac{x\rho}{\sqrt{1-\rho^2}}\right)$$

$$\times \exp\left(-\frac{x^2}{2}\right)dx - 1 = \frac{2}{\pi}\operatorname{atan}\left(\frac{\rho}{\sqrt{1-\rho^2}}\right)$$

$$= \frac{2}{\pi}\operatorname{asin}(\rho), \quad \text{(B.6)}$$

where Φ is the probability function

$$\Phi(x) = \frac{1}{\sqrt{2\pi}}\int_{-\infty}^{x} \exp\left(-\frac{u^2}{2}\right)du. \quad \text{(B.7)}$$

The last tree integrals in the right-hand side of Eq. (B.5) can be readily determined. Specifically,

$$pv\int_{-\infty}^{\infty}\int \frac{\theta_1}{\theta_2} e^{-(\sigma^2/2)(\theta_1^2+\theta_1\theta_2\rho+\theta_2^2)}d\theta_1 d\theta_2 = -\frac{2\pi\rho}{\sigma^2\sqrt{1-\rho^2}} \quad \text{(B.8)}$$

$$\int_{-\infty}^{\infty}\int e^{-(\sigma^2/2)(\theta_1^2+\theta_1\theta_2\rho+\theta_2^2)}d\theta_1 d\theta_2 = \frac{2\pi}{\sigma^2\sqrt{1-\rho^2}} \quad \text{(B.9)}$$

Substituting Eqs. (B.8), (B.6) and (B.9) into Eq. (B.5) one obtains

$$E[x_1x_2\,\operatorname{sgn}(x_3)\,\operatorname{sgn}(x_4)] = \frac{2}{\pi}\sigma^2\left[\rho_{12}\operatorname{asin}(\rho_{34}) + \frac{\rho_{13}\rho_{24} + \rho_{14}\rho_{23} - \rho_{34}(\rho_{13}\rho_{23} + \rho_{14}\rho_{24})}{\sqrt{1-\rho_{34}^2}}\right] \quad \text{(B.10)}$$